University of Twente

Faculty of
Electrical Engineering

Transducers Science and Technology

Master's thesis

Field emission and stability version 1.0

M.J.M. Koenders

1 October 2010

UNIVERSITY OF TWENTE

FACULTY OF ELECTRICAL ENGINEERING
TRANSDUCERS SCIENCE AND TECHNOLOGY

Field emission and stability

Master's thesis

1 October 2010

Author
M.J.M. Koenders

Supervisor
dr. ir. L. Abelmann

Graduation comittee
prof. dr. M.C. Elwenspoek
dr. ir. L. Abelmann
drs. A.F. Beker
ir. C.K. Yang
dr. ir. A le Fèbre

Contents

Chapter 1

Introduction

1.1 Introduction

In the recent years the interest in sub-micron and nano-electromechanical systems (NEMS) has grown significantly. Compared to micro-scale systems, nano-structures have higher sensitivity, lower power consumption and better mechanical characteristics. Traditional resistive and capacitive displacement detection techniques fail at nano-scale dimensions. External optical interferometry or magnetomotive techniques are used to readout the deflection of a nano-scale cantilever. [1]

An alternative sensing method which can be suitable for nano-scale dimensions is field emission. With this technique the field emission current is used to measures displacements between two conducting materials. The exponential relation between the emission current and the distance makes it an accurate and very sensitive sensor for small displacements.

For practical applications the unstable behavior of the field emission is the limiting factor and will greatly reduce the sensitivity and reproducibility of the measurements. Field emission sensing has been used in previous studies in pressure sensors [2], cantilever sensors [1] and positioning [3].

1.1.1 Field emission for cantilever sensing

To measure the deflection of nano-scale cantilevers traditional strain-gauges are almost useless because the generated signal is close to the thermal noise level. In an experimental study of Yang et al. field emission is used to determine the shift in the eigen-frequency caused by additional mass on the cantilever. In figure 1.1 a field emitter is shown which is integrated into the silicon wafer and constructed directly under a free-standing cantilever. The structure was made with the use of conventional MEMS technologies. [1]

1.1.2 Field emission for positioning

Field emission could also be used for high accuracy positioning. The emission current is used as a feedback signal for the positioning. Le Fèbre et al. introduced a new data-storage concept where data is stored in very small magnetic dots as shown in figure 1.1. A cantilever is used to read-out the polarity of the magnetic dot, which will correspond to the stored data. The cantilever is coated with a magnetic material and a field emitter at the end of the lever will measure the displacement caused by the magnetic field of the closest dot. [3].

For both concepts the stability of the emission current is very important.

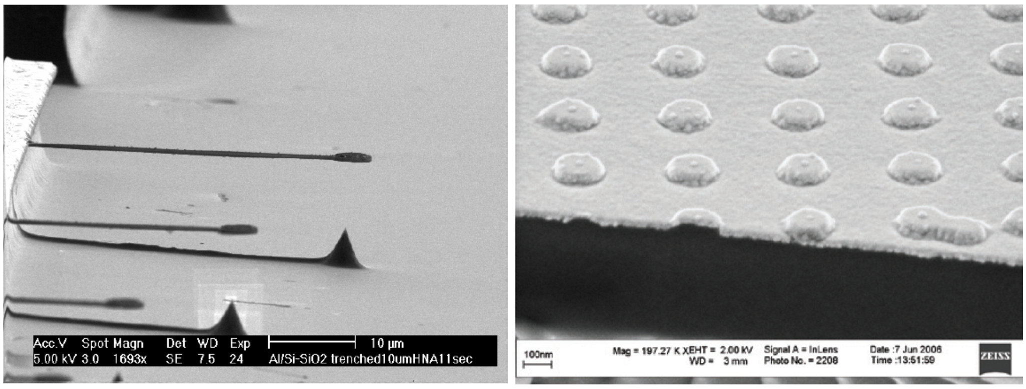

Figure 1.1: (left) Example of an integrated field emitter under a free-standing cantilever. [1] (right) New data-storage concept where field emission is used to read-out the nano-scale magnetic dots of data. [3]

1.2 Research goals

The goal of this research is to gain better insight in the possible causes of fluctuations in the field emission current. The approach is to investigate the effect of using different materials on the current stability. More information on the underlying causes for instability will enable us to design new and more stable field emission based measurement systems

1.3 Research organization

For six months this project took me to three locations across the Netherlands. Each location has its own expertise to contribute to the project.

The chair Electronic Instrumentation Labs at the University of Delft developed a micro-machining process to fabricate silicon tips with high aspect ratio. These high protrusion tips have a typical diameter of only ≈ 10 nm. The tip can be placed directly onto a fixed base.

At the University of Leiden, the chair of Interface Physics build a micro-scale manipulator with two piezo-stages. Both stages can be controlled individually inside a scanning electron microscope (SEM). This setup is used to attach carbon nanotube on top of the fabricated fixed tips.

Field emission measurements were done at the chair Systems and Materials for Information Storage at the University of Twente. They extended a commercial STM with a ultrahigh vacuum system, which enables them to do very accurate distance dependent field emission measurements under ultrahigh vacuum conditions. The facilities of the MESA+ cleanroom are used for thin-film deposition and ion implantation, both will be discussed in a later chapter.

1.4 Thesis organization

The outline of this thesis is as follows:

Chapter 2 starts with a brief history on the origin of field emission. From there the mechanism behind field emission is explained together with the mathematical equations of Fowler-Nordheim describing the field emission between two conductors. Furthermore the three key manifestations of fluctuations in the field emission are identified and the kinetics of surface diffusion are explained. The chapter ends with the explanation of the unique properties and synthesis of the carbon nanotubes which will later be used as field emitters.

In chapter 3 the experimental techniques are explained. Which are: (1) The fabrication of the high-aspect ratio field emitter tips; (2) The attachment of the carbon nanotube; (3) A description of the scanning tunneling microscope which will be used during the field emission measurements.

Chapter 4 uses the theory about surface diffusion to construct a particle model. This model is used to look at the influence of surface diffusion on the qualitative behavior of the field emission current and give more insight in the causes of the fluctuations of the emission current.

In chapter 5 the measurement results of different experiments are shows. These experiments are carried out with different kinds of field emitters, sample materials and tip-sample distances. In chapter 6 the results of the different setups will be discussed.

Finally in chapter 7 the conclusions of this work will be treated and recommendations for future work will be done.

Chapter 2

Theory

2.1 Field emission

2.1.1 Electron emission

The emission of electrons under high electric fields was first observed in 1897 by Wood [4]. In 1923 Schottky explained Wood's observations by assuming that electrons were jumping over the energy barrier, and he stated that the barrier could be lowered by an external electric field [5]. In the late 1920s Fowler and Nordheim published an article where they used quantum-mechanics to describe the tunneling of electrons trough the surface energy barrier, which explains the high emission currents measured at low temperatures [6]. The work of Schottky, Fowler and Nordheim showed that the emission of electron is dependent of the temperature of the emitter, the electric field and the work-function of the materials used.

The surface energy barrier of a metal-vacuum interface is shown in figure 2.1. The electrons are bound to the metal by this energy barrier and the distribution of energy levels of the freely moving electron follow the Fermi-Dirac statistics. For an electron to escape from the metal surface it has to overcome the difference in energy state in metal and the level outside the vacuum W_{vac}. For low temperatures the level of energy inside the metal equals the Fermi level W_F.

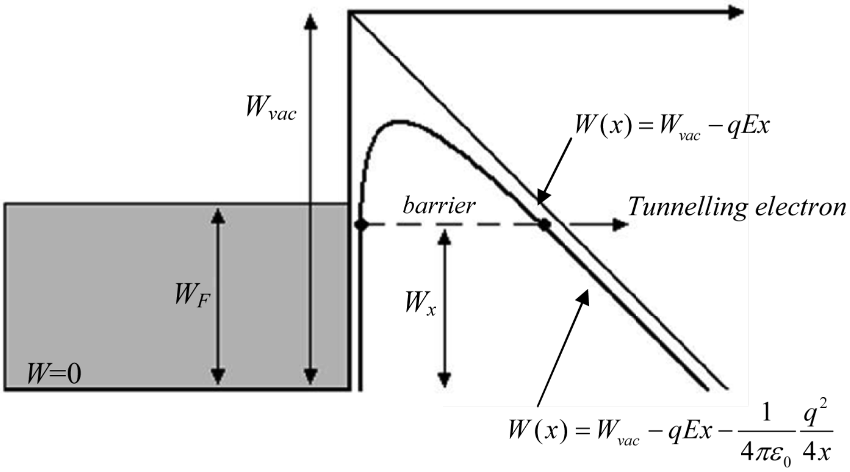

Figure 2.1: Schematic drawing of the surface energy barrier at metal-vacuum interface. The effect of an external field on the shape of the barrier is also shown. The vertical axis is the energy (W) and the horizontal axis is the distance (x) [7]

When an external electric field E is applied the vacuum energy barrier is reduced to a triangular shape described by equation 2.2. As is illustrated in figure 2.1 The electric field will reduce the barrier width, making it possible for electrons at Fermi level to tunnel through the barrier, this process is also known as cold field emission.

To complete the model of the surface energy barrier the electron image force has to be taken into account. The image force describes the attracting force on an electron at a finite distance of the surface of a perfect conductor, this results in equation 2.2. By applying an external field not only the width of the barrier but also the height is lowered due to image force. This effect is known as the Schottky effect. [7] [8] [3]

$$W(x) = \Phi - qEx \tag{2.1}$$

$$W(x) = \Phi - qEx - \frac{1}{4\pi\epsilon_0}\frac{q^2}{4x} \tag{2.2}$$

2.1.2 Fluctuations in field emission current

There are three major manifestations of the fluctuations of the emission current for field emission. These are shot noise, bistable telegraph noise and random fluctuations. [8]

Shot noise is the result of discrete nature of the electron and can be thought of as an irreducible minimum, that dominates the noise spectrum.

Bistable telegraph noise is a series of positive or negative pulses relative to a base emission level and appears to be due to the change between two or more states by individual atoms on the surface of the emitter. The inter spaced with periods of between transitions can be less then a second to more then 10 minutes.

Random fluctuations is due to the temporal change of the work function Φ or field enhancement factor γ of the emission surface caused by interaction of the surface with the operating environment or surface diffusion of the tips surface.

2.1.3 Fowler-Nordheim equations

Fowler and Nordheim used quantum mechanics to define the tunneling probability of an electron. From this probability function they derived the Fowler-Nordheim equation shown in 2.3. The equation relates the work-function and the electric field strength to the field emission current. [7]

$$I = K_1 A E^2 \exp\frac{K_2}{E} \tag{2.3}$$

Where E is the electric field, A is the area of emission, K_1 and K_2 are constants and Φ is the work function. Both constants are written in equation 2.4 and 2.5. Here m_e is the effective mass of an electron, q the electric charge of an electron and $\hbar$ is the Direc constant.

$$K_1 = \frac{q^3}{4(2\pi)^2\hbar\Phi} \approx \frac{1}{\Phi}\cdot\left(1.54\cdot 10^{-6}\frac{eV\cdot A}{V^2}\right) \tag{2.4}$$

$$K_2 = \frac{4\sqrt{2m_e}\Phi^{\frac{3}{2}}}{3\hbar q} \approx \Phi^{\frac{3}{2}}\cdot\left(-6.83\cdot 10^{9}\frac{V}{m\cdot eV^{\frac{3}{2}}}\right) \tag{2.5}$$

The electric field between two conducting plates is defined by equation 2.6. V is the potential between the plates and d is the distance between them.

$$E_{planar} = \frac{V}{d} \tag{2.6}$$

To show the relations between the current, voltage and the distance equation 2.6 is substituted into 2.3 and rewritten.

$$\begin{aligned} I &= AK_1E^2 \exp\frac{K_2 d}{V} && (2.7) \\ \ln(\frac{I}{E^2}) &= \ln(AK_1) - \frac{K_2 d}{V} && (2.8) \end{aligned}$$

From above equation three important relations can be concluded:

- The emission current I is exponentially related to the distance d under a fixed voltage V
- The voltage V is linearly related to the distance d under a fixed emission current I
- The emission current I is exponentially related to the voltage V under a fixed distance d

In figure 2.2 the exponential relations between the current and voltage at several distances are shown. For an increasing tip-sample distance the voltage between both has to be increased to maintain the same level of emission current. The right graph represents the linear relation between $\ln(\frac{I}{E^2})$ and $\frac{1}{V}$. This semi-logarithmic graph is also knows as the Fowler-Nordheim plot and its linear shape confirms that the measured current was caused by field emission instead of resistive contact. Both graphs are theoretical curves for field emission between two metal conductors in a vacuum environment for different distances 10 nm upto 50 nm tip-sample distance. [3].

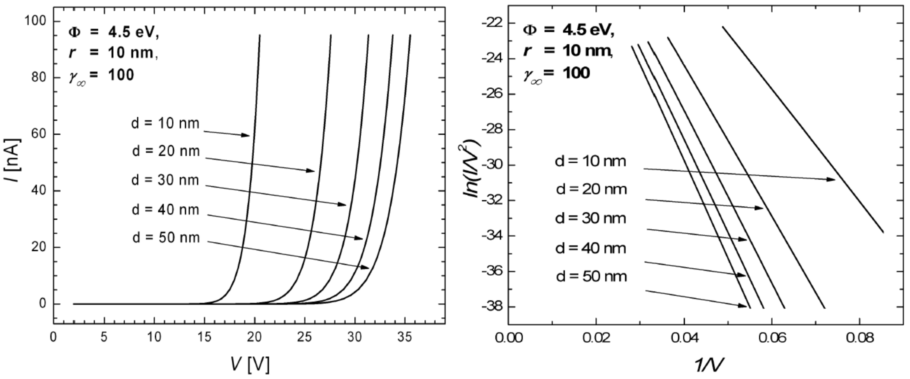

Figure 2.2: (left) Theoretical curve of the field emission current as function of the applied voltage for increasing tip-sample distances of 10,20,30,40 and 50 nm. (right) Semi-logarithmic representation of same curve to show the linear relation between I-V discussed in the Fownler-nordheim theorem. [3]

2.1.4 Field enhancement

Due to the geometry of the tip the local electric field close to the apex of the tip will be much higher than the calculated electric field used for parallel plate configurations in equation 2.6. The ratio between the true value of the electric field at the tip and the average macroscopic value is called the field enhancement factor (γ). This relation is shown in 2.9. le Fèbre states that the factor γ is strongly related to the tip geometry and the tip-sample distance. Less thickness and longer tip will increase the field enhancement factor. [9].

$$E_{local} = \gamma E_{planar} = \gamma\frac{V}{d} \tag{2.9}$$

2.2 Surface diffusion

2.2.1 Surface diffusion mechanism

There are a variety of mechanisms that contribute to the diffusion of particles in solid material. Diffusion caused by hopping or jumping of adatoms is probably the best known cause of surface diffusion. Adatoms are located on adsorption sites between the lattice of the surface material. Each adatom vibrates and attempts to overcome an energy barrier E_D to jump to a neighboring absorption site. The height of this barrier is defined by the orientation of the surface lattice, the strength of the surface-adatom bond and interaction with other species present on the surface. The rate of the diffusion is strongly influences by the surface temperature. An increase in the surface temperature will increase the activity of the adatoms and this will increase the surface diffusion, the adatoms will gain more energy and the probability they overcome the energy barrier increases. In figure 2.3 the relation between the surface temperature and the diffusion rate of lead (Pd) adatom on a tungsten (W) surface is shown. This plot is also known as the Arrhenius plot. [10]

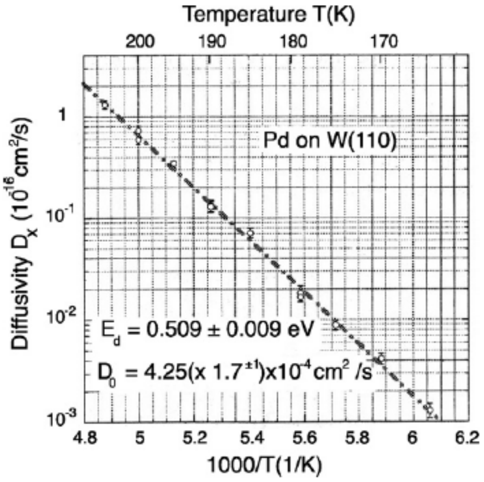

Figure 2.3: Arrhenius plot, showing the influence on the diffusivity of Pd adatoms on Tungsten surface [100] for a increasing temperature. [10]

Another mechanism contributing to the total surface diffusion is atomic exchange. In atomic exchange an adatom changes position with an atom from the solids lattice. The removed atom will become an adatom itself and diffuse across the surface. Another mechanism is based on quantum tunneling effects and known as tunnel diffusion. Instead of overcoming the energy barrier particles tunnel trough this barriers. In vacancy diffusion adatoms diffuse along the surface between vacancies in the surface lattice. In this report the focus will be on the jumping mechanism because it has the largest contribution on the diffusion and movement of the adatoms across a surface. [10] [11]

2.2.2 Surface diffusion kinetics

The surface diffusion mechanism is build up out of three components: (1) The direction of the adatom jump (2) The jumping rate (3) The length of the adatom jump. The jumping rate describes the rate at which an adatom attempts to jump to an adjacent side. The length of the jump is defined by an probability distribution. The direction of the jump is chosen randomly. These three key components will be used later as an foundation for the surface diffusion model. Each component will be highlighted in more detail.

The jump rate of adatoms

The diffusion of the adatom is described by the material parameter D and the concentration gradient along the x-axis $(\delta c/\delta x)$. The adatom flux J in one-dimension is given in equation 2.10.

$$J = -D\frac{\delta c}{\delta x} \tag{2.10}$$

The diffusivity D is given by the standard Arrhenius relation shown in equation 2.11.

$$D = D_0 \exp(-\frac{E_D}{kT}) \tag{2.11}$$

In equation 2.12, v_0 describes the vibration frequency of an adatom. Each cycle the adatoms attempts to hop to an adjacent absorption site. Depending on the material of the adatom this frequency lies at $\approx 10^{-12}s^{-1}$. l is jumping length, S_D and E_D are respectively the entropy and activation energy for the diffusion.

$$\begin{aligned} v_0 &= v\exp(\frac{S_D}{k}) & (2.12) \\ D &= v_0 l^2 \exp(-\frac{E_D}{kT}) & (2.13) \end{aligned}$$

The term $exp(-E_D/kT)$ in equation 2.13 can be interpreted as the probability that a jump attempt of a particles succeeds. The Boltzmann constant k is a constant value, the change of a successful jump depends on the activation energy E_D and the surface temperature T. [10] [12]

The jump length and directions of adatoms

The traditional view of surface diffusion is that adatoms randomly jump between nearest-neighbor absorption sites. Through field ion microscopic observations this picture changed. Adatoms are also able to jump to non-nearest neighbor absorptions sites, which could be several sites away. Senft et al. observed the diffusion of lead (Pd) on a tungsten (w) surface and recorded the size of the jumps of hundreds of adatoms during several seconds. The result are shown in figure 2.4. To illustrate the impact of the surface temperature on the frequency and size of the adatoms jumps the experiment was done for a surface temperature of 122 K (left) and for 133 K (right).

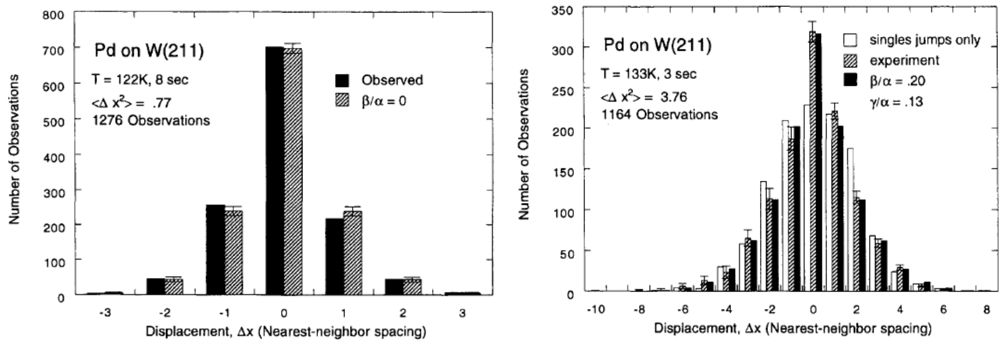

Figure 2.4: The distribution of the displacements for lead (Pd) adatoms on a tungsten W surface with surface temperatures of 122 K and 133K. The increase of temperature will increase the probability for larger steps. [13]

When the temperature is elevated the adatoms become more energetic and the frequency of long-jumps increases. As can been seen in the right figure of 2.4 larger jumps are observed when the sample is heated to 133 K. At a certain point the long jumping adatoms will dominate the diffusion process. [13]

2.3 Carbon Nanotubes

Graphite is the ground state for a huge number of carbon atoms like diamond, carbon and methane gas. In figure 2.5 a section of a 2D graphene sheet is shown. This small 2D sheets of graphene consists out of benzene-type hexagonal rings of carbon atoms. The edges of the sheet still have a lot of free bounding energy. To avoid occurrence a small number of carbon atoms will close the shell and form nano-structures such as fullerenes and carbon nanotubes. [14]

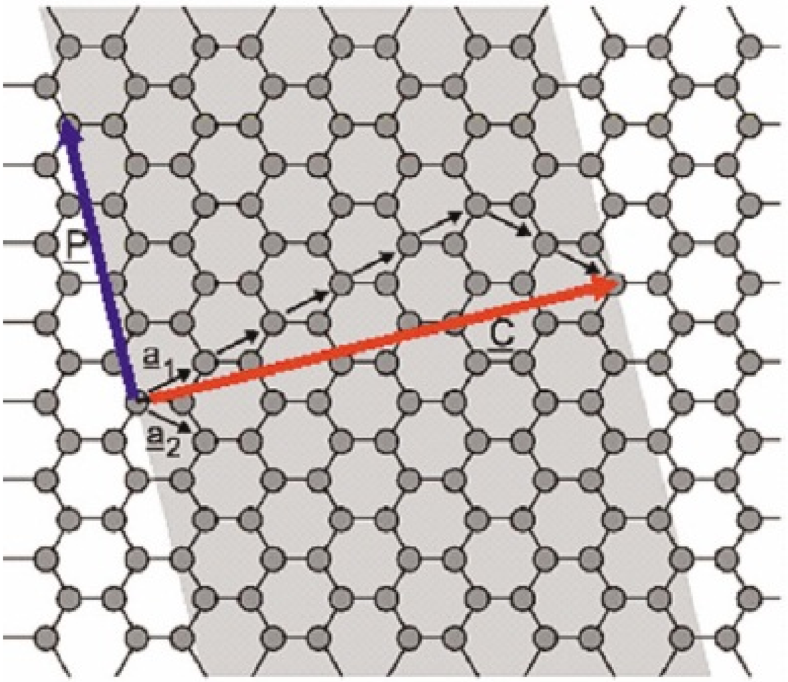

Figure 2.5: Schematic drawing of a flat 2D graphene sheets, which consists out of benzene-type hexagonal rings of carbon atoms. Nanotube can be created to fold the sheet along one of the three lattice vector (m,n) which describe the diameter and charility of the resulting nanotube.[15]

A single-walled carbon nanotube (SWNT) is formed by rolling a sheet of graphene into a cylinder along a lattice vector C(m,n). This vector describes all possibilities of connecting two crystallographically equivalent sites of the two-dimensional graphene sheet of each other to form a cylinder. The lattice vector is given by: $C(m,n) = na_1 + ma_2$, where a_1 and a_2 are the unit vectors of the hexagonal lattice as shown in figure 2.5. The structure of any CNT is described by this pair of integers (m,n). [15]

In other words the vector itself describes the chirality of the tube. The chirality is the angle between the hexagons in the graphene sheet and the axis of the tube. The length of the lattice vector correspond with the resulting diameter of the nanotube. Both have a significant influence on the electrical behavior of the nanotube, which will be discussed in more detail later.

As shown in figure 2.5 there are three possibilities to fold the graphene sheet. The lattice vectors $(8,8)$, $(8,0)$ and $(10,-2)$ will form nanotubes with respectively arm-chair, zigzag and charil configurations. The three different types of nanotube are shown in figure 2.6. Depending on the size of the vector SWNT can have extra-ordinary small diameters of 0.7 nm, but still be surprisingly strong. The young modulus of a single walled nanotube lies around 1 TPa and the yield strength can be as large as 120 GPa. [16] [17].

A multi walled carbon nanotube (MWNT) is a stack of graphene sheets rolled up into a multi-layer cylinder. The sheets can be ordered parallel or have a piled cone structure. The diameter of a MWCNT are typically $15-50nm$ and are several microns long. The techniques to fabricate multi-wall nanotubes

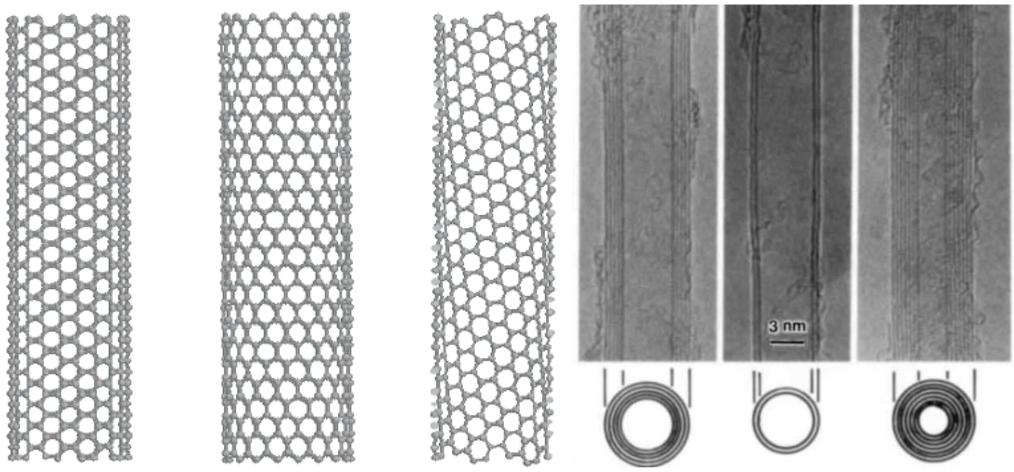

Figure 2.6: (left) Folding of the lattice vectors $(8,8)$, $(8,0)$ and $(10,-2)$ will result in three different oriented nanotubes, these configurations are respectively called armchair, zigzag and chiral tubes. [17] (right) TEM image of the cross-sections of three different MWNT. From left to right you will find a MWNT of five parallel layers with a diameter of $(6.5nm)$, two parallel layers $(5.5nm)$ and one of six parallel layers $(6.7nm)$ [18].

are similar to single-wall only they make use of a different catalyst. For SWNT usually iron is used as a catalyst and for MWNT nickel is used. In figure 2.6 shown of the cross section of three MWNT with a different number of layers. In this experiment MWNT be used as field emitters. [14] [16]

2.3.1 Electrical properties

The lattice vector described how the graphene sheet folds into a nanotube, but this vector also tells us what happens at the end of the sheets when they get attached to each other. Depending on the chirality the resulting nanotube will have metallic or semiconductive properties. It can be shown that for a lattice vector (n,m) where $n = m$ the nanotube is metallic. The nanotube has a small bad gap when $n - m = 3i$, where i is an integer. When $n - m \neq 3i$ then the nanotube has semiconductive properties. The length of the lattice vector in other words the diameter of the tube will have inverse proportional relation with the band-gap of the semiconductive nanotube. [15]

Metallic

Transport of electrons in conductive materials are limited by the defects in the lattice of the material. The scattering of carriers against defects will slow this process. The quality of transport is measured in the length of the mean free path. An example of a metallic carbon nanotube is the armchair nanotube. Because of the perfect hollow cylinder structure there is no scattering at the materials boundaries. Also the lattice of the graphene sheet is flawless, which can results in an incredible free mean path up to 10 μm. The conductivity of a nanotube can be as much as eight times higher than that of copper. Nanotube can carry current densities exceeding $10^9 \frac{A}{cm^2}$. Nanotube are extraordinary conductors, with low-resistivity and low-losses. Therefor the nanoscale chip industry has a lot of interest in these tubes for interconnects on nanoscale chips. [19] [15]

Semiconductor

The semiconductive CNTs have a band gap E_g which is inversely proportional to the diameter of the nanotube. Semiconductive CNTs possibly will be used in future field-effect transistors called CNT-FETs. [19]

2.3.2 Fabrication

Throughout the years different method of synthesis CNTs have been developed. The three most used fabrication techniques are laser ablation [20] , arc discharge [21] and chemical vapor deposition (CVD) [22]. The multiwall carbon nanotubes used in this experiment are producess with arc discharge this technique will be treated briefly.

Arc discharge

Arc discharge is based on the use of two high purity graphite electrodes, which are positioned opposite to each other. A schematic drawing of an arc discharge setup in shown in figure 2.7. A large DC current with an alternating AC current is applied across the cathode and anode electrode. This will produce a gray lighted shell named the soot. The intense heat generated by the discharge will cause the carbon electrodes to vaporize at a rate of $1 mm/min$. The vaporized carbon molecules will cluster and self-assemble in the core of the soot to for all different kinds of nanostructures. The created by-product will be removed in a later process.

To produce pure SWNT the materials used in this process have to be of high purity to. This makes this technique quite expensive. During synthesis there is very little control on the diameter of the nanotubes. New technique like arc-in-liquid discharge are developed, here the arc discharge is carried out inside a liquid. This method makes is possible to synthesis carbon nanotube at low temperature. Better controlling of the diameter and length of the nanotubes. Furthermore the requirements on the purity of the used materials are much lower. [21]

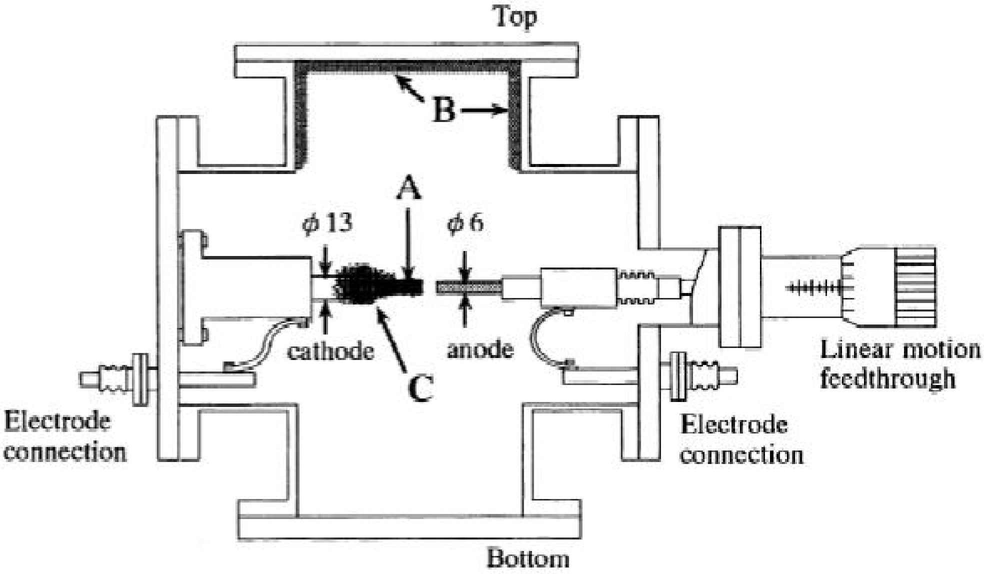

Figure 2.7: Schematic drawing of an arc discharge setup, here a large DC current is applied to the graphite electrode (anode and cathode). Due to the arc discharge the electrode will evaporate and the loose particles will reassemble itself into carbon nanostructures near the cathode. The reaction chamber is usually filled with argon or helium gas. [21]

Chapter 3

Experimental techniques

3.1 Micromachining silicon high-aspect ratio tips

The department of Microelectronics at the Technical University of Delft has developed High-Aspect Ratio (HAR) tips with a fixed base. The tips are used to investigate the use for field emission based nano-sensor for nano electro mechanical systems (NEMS). As explained in the theory the field enhancement factor depends on the geometry of the tips, during fabrication the goal is to make long but thin field emitters. In our research the HAR tips are used as field emitter inside a Scanning Tunneling Microscope (STM). The STM will be treated later in this chapter.

The process for making the fixed tip has been designed and improved by C.K. Yang of the University of Delft. The tips fabricated by this process are typically 2-3 μm high and have a tip radius of 10-25 nm. SEM images of the tips are shown in figure 3.2 and 3.3. The fabrication process will be discussed briefly.

First a layer of 311 nm SiN is deposited onto a 4" standard silicon wafer (a). Two patterns are used to create the base and tip mask. The SiN is etched down with a CHF_3 plasma etching process. Afterwards the full wafer is etch 300 μm deep in KOH, this will form the tip bases and dices structure of the wafer (b). Again a CHF_3 plasma is used to etch the SiN layer for $\approx$ 155 nm until only the tip mask remains. Isotropic etching with a SF_6 plasma is used to make a start of the tips shape (c). The Si layer is etched anisotropically further with a SF_6 and O_2 plasma to increase the height of the tip. During these last two steps the top of the tip is protected by the SiN layer. Again an isotropic etch is used to further sharpen the tip (d). The Si layer on top of the wafer is oxidized to form a 544 nm tick SiO_2 layer (e) to protect the structure during the next steps. The complete structure is turned up side down to remove the SiN layer and reduce the thickness of the Si tip (f). To remove the remaining SiO_2 and the SiN tip mask at the front side the wafer is submerged in HF for several minutes. The final step is to clean the wafer with demineralized water.

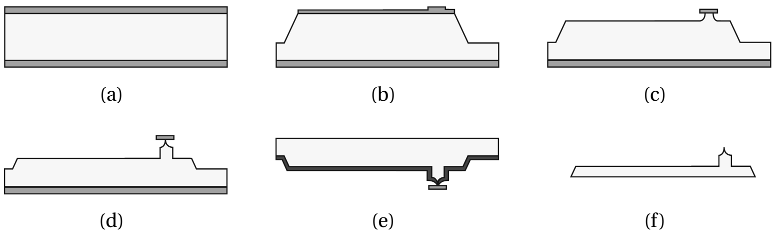

Figure 3.1: Selection of steps of the fabrication process of the high-aspect ratio tips.

The main advantage of this process is that two masks are used to create a single masking layer. This saves one deposition step and solves the photoresist spin-coating problem after etching the first mask for the base and the second mask has to be applied. The fabricated tips can be process further to coated them with a thin layer of metal to make them conductive. The complete process document with all the 12 steps to fabricate the HAR tips can be found in the appendix A.

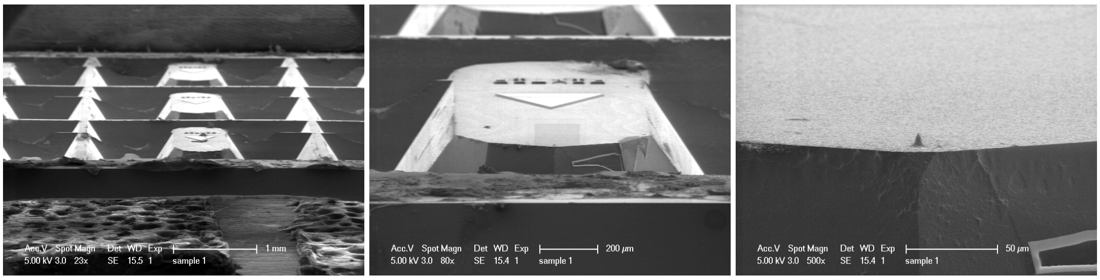

Figure 3.2: SEM pictures used for inspection of one batch with 16 high-aspect ratio silicon tips. These tips were fabricated in the cleanroom at the Technical University of Delft

3.2 Hydrophobic and hydrophilic tips

On every solid material is a microscopical layer of water present on the surface. The binding energy of water is lower than that of the metal surface, the thin film of water will lower the total binding energy between adatoms and the metal surface. The lover binding energy will increase the probability for an adatom to jump to an adjecent site, this will increase the diffusion rate. To study the effect of the water layer on field emission, hydrophilic and hydrophobic emitters are needed. To create tip with hydrophilic properties a thin metal film of molybdenum is deposited onto the silicon tips. Silicon is by nature hydrophobic but is a bad conductor. Therefore the silicon tips are doped with boron ions to lower the electrical resistivity and make the doped silicon tips suitable as field emitters. The fabrication process of both tips will be discussed further.

3.2.1 Thin film deposition of molybdenum

To lower the resistivity of the silicon tips a thin layer of metal is deposited onto the silicon surface. Important here is to use sputtering technique to deposit the metal layer, this technique has a good step coverage and will ensure us that the sides of the tip are covered. The sputtercoater "Sputterke" at the MESA+ institute is used to deposit a layer of 50 nm molybdenum onto two sets of 16 silicon tips. The setting of this process can be found in table 3.1. Molybdenum is a noble metal and has a natural high resistance against oxidation, a hydrophilic character, a high melting point and strong bounding energy. Other noble metal like platinum or tungsten can also be used, but experiments show that molybdenum results in the most stable emission current [3].

Table 3.1: Deposition parameters used for sputtering 50nm of thin metal film of molybdenum on the silicon tips.

gun	tickness (nm)	argon	pressure	pressure system	power (W)	time (mm:ss)
Mo	50	81.8	$6.6\cdot10^{-3}$	$1\cdot10^{-6}$	200	04:00

3.2.2 Highly doped silicon tips

Silicon is a hydrophobic material by nature but is a bad conductor. To keep the hydrophobic character and increase the conductivity of the silicon, the material can be doped with either boron or phosphorus

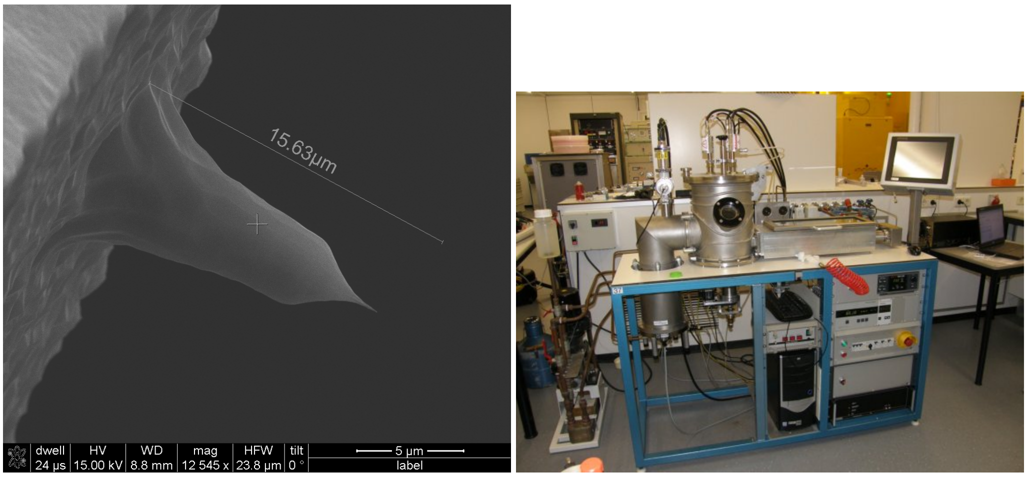

Figure 3.3: (left) High aspect ratio silicon tip coated with a 50 nm conducting thin layer of molybdenum. (right) Sputtercoater "sputterke", used for deposition of thin films by sputtering.

ions. There are doped silicon wafers on the market. But it cannot achieve high conductivity. Another method to create metal-like silicon has to be found.

The solution is to use ion implantation to dope a set of 16 silicon tips with boron ions. The tips are glued with photo-resist onto a standard 4" wafer and placed inside the ion implanter. Boron ions are accelerated with a voltage of 500 KeV towards the silicon wafer. The boron ions hit the wafer with great speed and the ions will settle in the silicon crystal structure. The process of implanting took around half a hour and the concentration of boron ions lies around $1 \cdot 10^{15}$ ions per cm^3, this corresponds to a resistivity of $\approx 10\,\Omega cm$.

The boron ions are implanted in the silicon crystal structure, but still have to be activated to be adopted in the silicons crystal structure. To generate enough energy for this activation the sample is annealed at high temperature. With the help of a rapid temperature annealer the substrate is heated to 900 degrees for 10 seconds. To minimize the change of unwanted growth of silicon-oxide (SiO_2) during operation a constant flow of nitrogen gas (N_2) will stream over the substrate.

The result should be a conducting tip which preserved its hydrophobic characteristics. Despite of our precautions during the implantation process a silicon-oxide layer had grown on our tips. SEM images of the unwanted silicon-oxide layer are shown in figure 3.4. Unfortunately this oxide layer insulates the tips and field emission from these tips was not possible.

3.3 Attachment of Carbon Nanotubes

The group Interface Physics at the University of Leiden developed a manipulator which can be controlled inside an Scanning Electron Microscope (SEM). The manipulator has two computer controlled piezo-stages with three degrees of freedom. This enables us to move two individual object with nanoscale steps, the movement of both objects can monitored with the electron microscope. This setup is shown in figure 3.5 and will be used to place the carbon nanotube on top of to the silicon tip.

In previous work done by Jeroen de Vries and Anne-France Beker the long nanotubes were shortend by breaking them into two parts with the use of a high current, this made them have a open cap structure. In their attempts they were unable to produce a stable field emission currents from these open cap nanotube [23]. Rinzler et al. experimentally proven that closed cap are more stable then open cap nanotube [24].

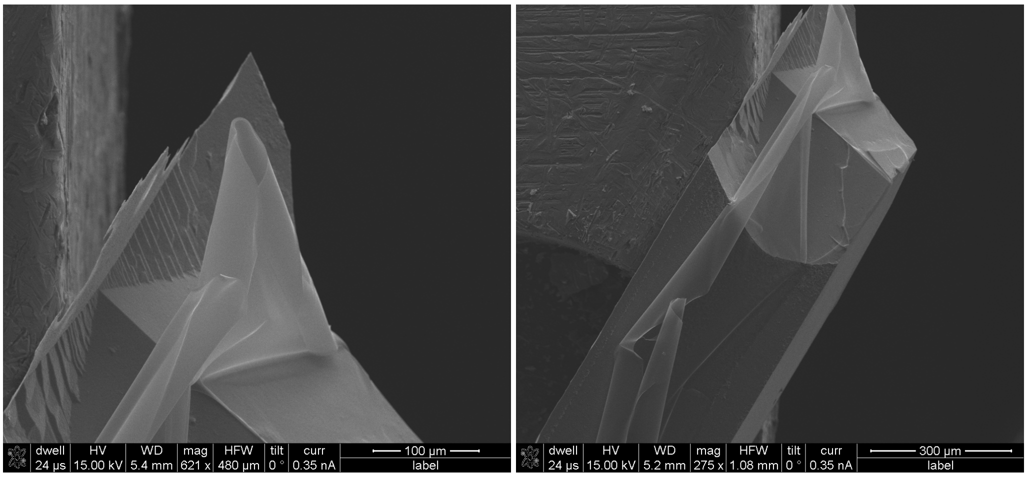

Figure 3.4: Unwanted growth of a thin layer of SiO_2 during the the ion-implantation process.

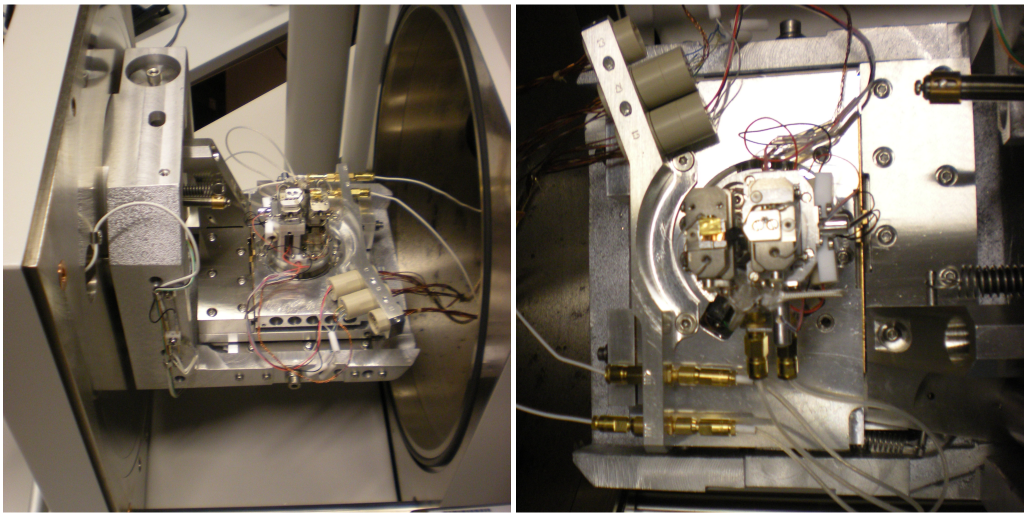

Figure 3.5: The manipulator specially designed to work inside the SEM. The manipulator has a coarse and a fine stage.

From the company Rosseter Holdings Ltd. short multiwall nanotubes were bought. This company uses the arc-discharge technique to synthesis the nanotubes. This method produces a mixture of carbon nano-particles and MWNT's. Length and diameter are distributed by three type with maximum of 200, 300 and 500 nm for lengths, 6.5, 12 and 20 nm for outer diameters. The mixture of carbon structure is stuck to a small piece of carbon tape. This tape is placed onto the coarse piezo stage. A special AFM tip sample holder is made to clamp the tip into the holder which can be placed onto the fine stage. The chamber of the SEM is closed and pumped down until the vacuum is low enough to operate the electron microscope. [25]

The coarse stage with the carbon tape containing the nanotubes is navigated near to the tip. Then the fine stage is moved towards a spot on the tape where an carbon nanotube is located. The SEM is used to align the tip with the nanotube in the x-direction and y-direction. By changing the focus point of the SEM, the alignment of the nanotube and silicon tip in the z-direction can be determined.. When the tip is brought close to the nanotube it will stick due to Van de Waals forces. The contamination present in the vacuum environment and at the surface of the tip are used 'glue' them together. The scan area of the SEM is adjusted to only cover the area where the nanotube is touching the tip. The highly energetic electrons which are shot toward the object will hit carbon atoms present in the vacuum or surface and will bound to the tips surface, thereby connecting the tip with nanotube mechanically and electrically.

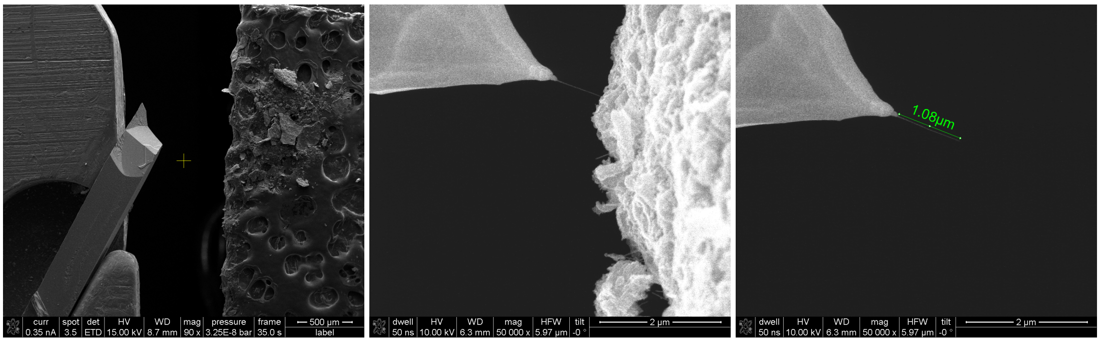

Figure 3.6: Three SEM pictures taken during the attachment of a carbon nanotube on a high-aspect ratio silicon tip. (left) alignment of tip and carbon-tape with CNT's on it. (middle) Attachment of CNT and retracting the CNT slowly from the carbon-tape (right) the silicon tip is extended with a 1.08 μm carbon nanotube

In some cases the Gas Injection System (GIS) is used to deposit a small layer of platinum to increase the strength and conductivity of the connection. The electrical connection between the tip and the attached CNT is tested afterwards by applying a small voltage onto the tip and the nanotube before carefully pulling the tube out off the carbon tape. In figure 3.6 a series of SEM pictures are shown taken during the attachment of a nanotube to the tip and safely pulling it out of the carbon tape.

3.4 Measure field emission currents

3.4.1 Measurement setup

At the group of Systems and Materials for Information storage group (SMI) at the University of Twente a commercial STM from RHK Technology is available. With this measurement setup we are able to measure field-emission as an effect of tip-sample displacement with great precision. To reduce the effect of adsorption of residual gas atoms on the emitter surface, A. le Fèbre extended the STM with a custom build ultra-high vacuum system. Also custom tip-holders were developed to make it possible to mount silicon tips with an AFM-base in the STM.

The RHK STM uses a beetle-type scan-head. The scanner consists of three piezo electric legs and stands on top of the sample holder. The scanner uses stick-and-slip motion technique to move in the X, Y and Z directions. Another piezo element present at the tip-holder enables it to move in the Z-direction for about 200 nm. A schematic drawing of the STM is shown in figure 3.7 here the scanner head and sample holder are shown. The scan-head can scan a maximum area of 5 x 5 μm. The movement and lowering of the tip towards the sample is controlled by the RHK SPM1000 control system and takes care of all actuation and data-acquisition.

All measurements are carried out in UHV and therefore an additional UHV system consisting of a scroll pump, turbo pump and an ion pump are installed. The combination of these three pump allows us to reach a vacuum of 5×10^{-9} mbar. This process takes up to several hours. The storage elevator is used to pre-load extra tips and sample, which can be measured later in the same vacuum. The changing of the tips and samples is done with the wobble stick which is shown in figure 3.7. In figure 3.8 a press-photo is shown of the STM setup. Look closely inside the chamber to see the scan-head standing on top of the sample-holder.

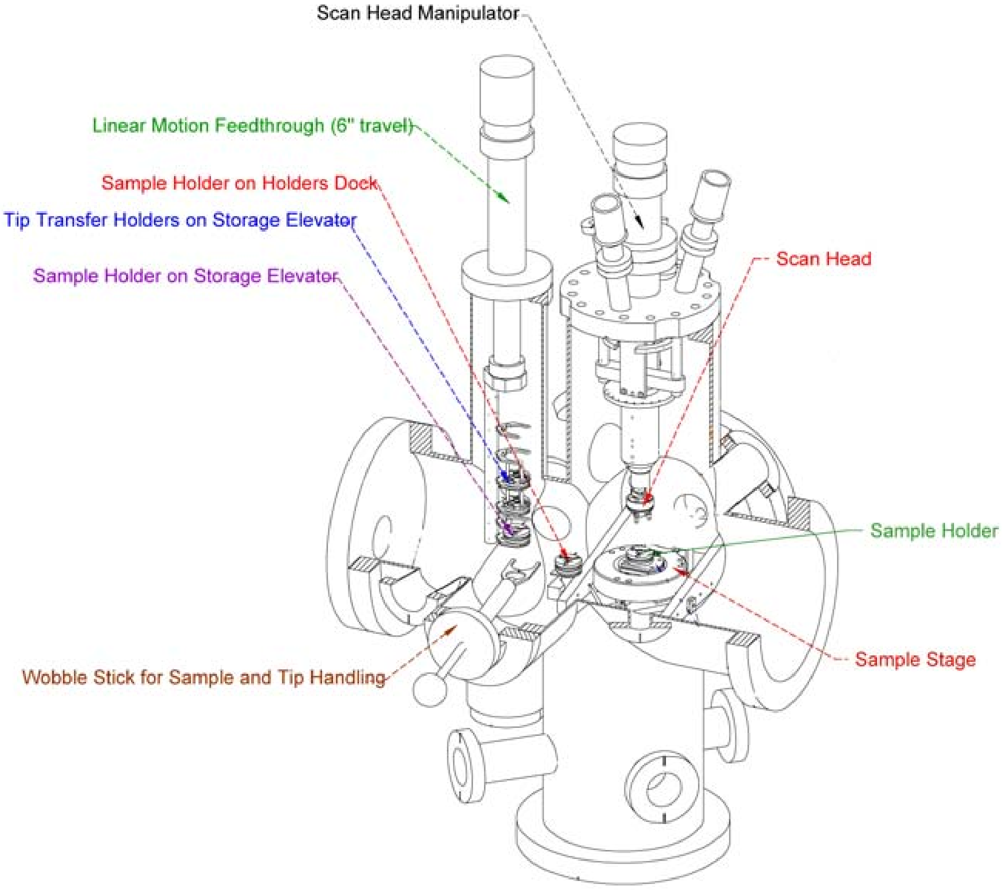

Figure 3.7: Schematic drawing of the RHK 300 system showing the main components of the used STM instrument. [26]

3.4.2 Labview to measure emission current

The RHK software is used for positioning of the tip at a certain tip-sample distance. Instead of using the SPM1000 a Keithley 6497 pico-ampere meter and high voltage source is used. This measurement device has a much higher sensitivity and dynamic range from 20 mA down to 10 fA at 1000 readings per second and can supply up to 500 Volts. Another big advantage is the ability to directly control the Keithley from our own custom build Labview applet. Le Fèbre already made a Labview program to perform distance dependent I-V measurement. This program was extended to perform stability measurements for different parameters. A screenshot of the labview workspace and the customized control interface are shown in figure 3.9. [27] [3]

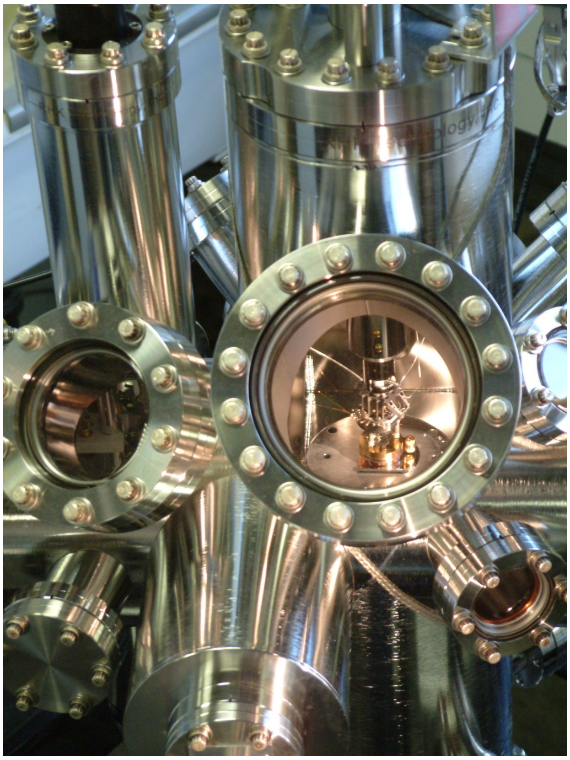

Figure 3.8: Picture of the STM measurement setup. Look closely inside the chamber to see the scan-head standing on top of the sample holder.

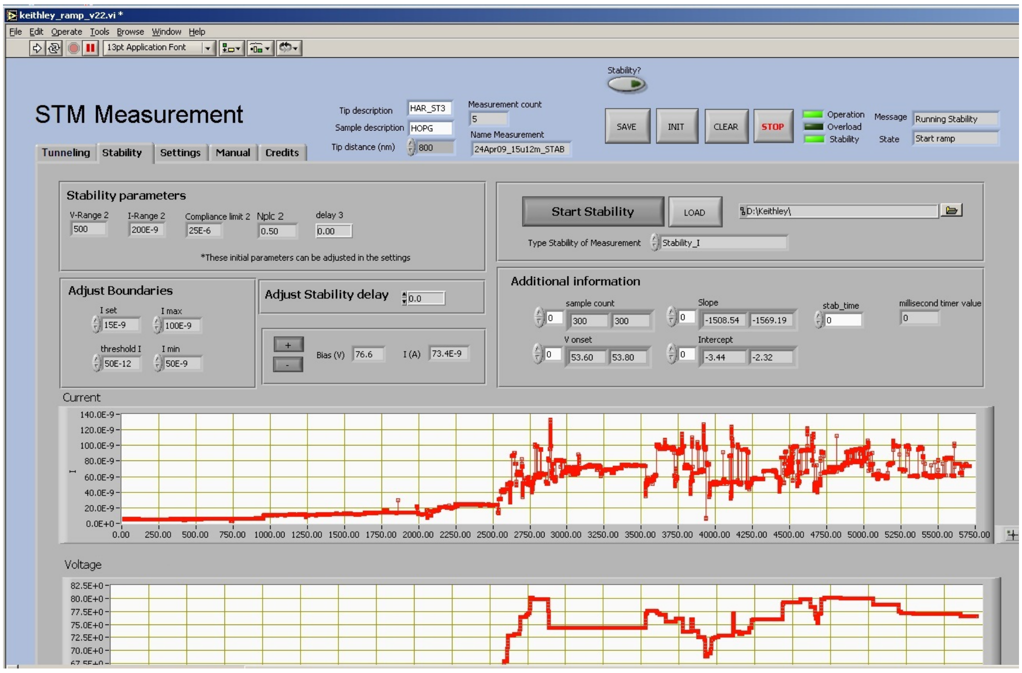

keithley_ramp_v22.vi *

STM Measurement

Tip description HAR_ST3
Sample description HOPG
Tip distance (nm) 800
Measurement count 5
Name Measurement 24Apr09_15u12m_STAB
Message Running Stability
State Start ramp

Stability parameters
V-Range 2 500
I-Range 2 200E-9
Compliance limit 2 25E-6
Nplc 2 0.50
delay 3 0.00
*These initial parameters can be adjusted in the settings

D:\Keithley\
Type Stability of Measurement Stability_I

Adjust Boundaries
I set 15E-9
I max 100E-9
threshold I 50E-12
I min 50E-9

Adjust Stability delay 0.0

Bias (V) 76.6
I (A) 73.4E-9

Additional information
sample count 0 300 300
V onset 0 53.60 53.80
Slope 0 -1508.54 -1569.19
Intercept 0 -3.44 -2.32
stab_time 0
millisecond timer value 0

Figure 3.9: Screenshot of the Labview program used to control and show the measured signal during stability measurements. The applet automatically conduct several stability measurements for different levels of current.

Chapter 4

Numeric model of surface diffusion

4.1 Create a surface diffusion model

4.1.1 Particle-system simulation methods

There are several methods to simulate and study surface diffusion. These methods extend from picoseconds up to nano- and microseconds scales where phenomena like island diffusion and thin film growth. One of these methods is the Monte Carlo method which is a stochastic technique to investigate particle systems.

To apply this simulation technique the surface of the diffusion system is mapped to a discrete squared lattice. All the possible absorption sites get their own coordinates. Instead of using the interactions between all atoms to calculate the movement, a combination of the attempt frequency in equation 2.12 and the step-size probability distribution from figure 2.4 is used. As explained in the theory it is possible for an adatom to make jumps larger then unity. The use of the probability distribution decreases the computational time needed to simulation the diffusion of adatoms. [11] [12]

4.1.2 Assumptions made in the model

Some assumptions are made which keep the model simple. The assumption will have influences on single adatoms, but little on the characteristics of the overall diffusion.

List of assumptions made in the diffusion model.

- No attraction or repulsion between adatoms, atoms in the lattice or other species on the surface lattice.
- No cross-channel diffusion of adatoms. Due to the lower energy barrier of in-channel movement it dominates the diffusion process. Only at high temperature cross-channel diffusion occurs.
- Ignore orientation of the surface lattice. Close packed surfaces like [111] have higher diffusion rates than of an open structure [100].
- Macro scale movement of clusters of adatoms are ignored. Adatoms cannot form groups and move together.
- Atom exchange between adatom and atoms from the surface lattice are not possible. Also possible vacancies in the lattice of the surface are not implemented.

4.1.3 Modeling in NetLogo

Netlogo is used to create our adatom diffusion model. NetLogo is a programmable modeling environment for simulating particles systems. NetLogo is suited to model complex systems which develop over time and enables the programmer to give thousands of ’agents’ instructions and operate independently in a huge macro system. Netlogo also has a built-in feature to export the model to a java applet, which can then easily put onto the web to share the model with fellow scientists. [28]

The diffusion model can be found online at:
http://home.student.utwente.nl/m.j.m.koenders/thesis/model/surface_diffusion.html
Also a model is created to simulate diffusion of gases particles:
http://home.student.utwente.nl/m.j.m.koenders/thesis/model/gas_diffusion.html

4.1.4 Interface, graphs and controls

In figure 4.1 a screenshot is shown of the interface of the diffusion model during operating. The controls on the left side are used to set all parameters and control the process during simulation. The black square in the middle is the actual surface area with the adatoms jumping around. On the right are several graphs monitoring the amount of particles in the system, the step-sizes of all adatoms, the concentration of adatoms along the x-axis and more.

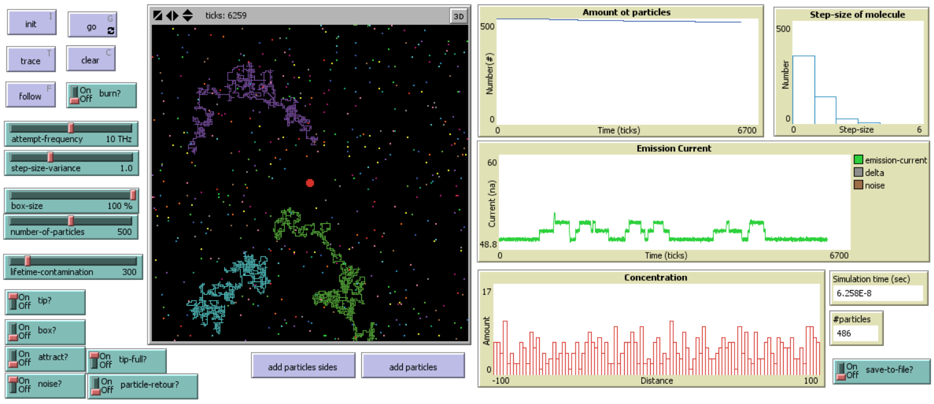

ticks: 6259
attempt-frequency 10 THz
step-size-variance 1.0
box-size 100 %
number-of-particles 500
lifetime-contamination 300
Simulation time (sec) 6.258E-8
#particles 486

Figure 4.1: Screenshot of the interface of the model to simulate the impact of surface diffusion on the emission current.

Below are all the control buttons and there functionality are explained:

- **init**, to initialize the simulation and place certain amount of adatoms randomly across the simulation area.
- **go**, to start the simulation. During operation this button can also be used to pause the process.
- **trace**, to trace the path of a single adatom. This button can be pressed multiple times to trace more adatoms.
- **follow**, to highlight and follow one individual adatom over time.
- **add particles**, during simulation extra adatoms can be added at a random place.

Next all configurations options are explained briefly:

- **attempt-frequency**, set the frequency for each period a adatom tries to jump.
- **step-size-variance**, set the variance of the normal distribution to determine the step-size of each adatom.
- **box**, if turned on a surrounding box will be drawn around the borders to close the system.
- **box-size**, determine the size of the box which is drawn.
- **number-of-particles** determine the number of particles which are added during initialization.

Initialize surface and adatoms

During initialization a certain amount of adatoms are placed randomly across the simulation area. On each absorption site can only be one adatom present. If the spot is already taken it searches randomly until it has found a empty spot to place the adatom. The tip area is drawn in the middle of the workspace. The workspace can be made smaller by using the box-mode. Depending on the value of the box-size, a box is drawn in the workspace and limits the active area where adatoms can move freely.

The jumping process

First the direction in which the adatom is heading is determined for each particle. Since our surface has a square lattice, the adatom can either head north, east, south or west. The directions are chosen randomly from this set.

The next step is to determine the size of the jump for each adatom. This size of this jump can also be zero, which means the adatom stays at its current position. Based on figure 2.4 the probability of the size of the steps is chosen to be normal distributed. Increasing the step-size-variance in the settings will increase the average step-size of the adatoms. During the simulation the step-size-variance can be changed. The effects of a change can immediately been seen by the change in activity of the adatoms.

The last step before the adatom is moved to its new location is to look if target absorption site is still available and not occupied by another adatom. When another adatom is present the adatom cancels the jump and stay at its current position. An adatom with the intention to move across the borders of the simulation area is placed back on the opposite side of the simulation area. In figure 4.2 a screenshot is shown from the simulated surface where the movements of three adatoms are traced. In this image can clearly be seen the random walk character of the particles along the surface.

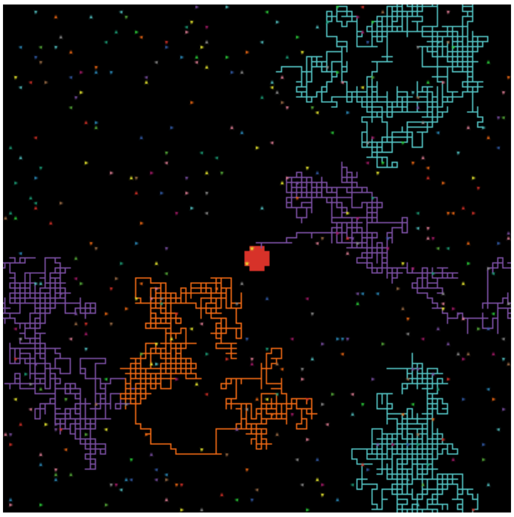

Figure 4.2: Screenshot of the simulated square lattice surface where adatoms are jumping around. The movement of three adatoms is traced to highlight their journey across the surface. The red 'circle' in the middle illustrated the area of the tip

Extending the surface diffusion model

The surface diffusion model is extended to investigate the influence of surface diffusion on the stability of field emission currents from field emitters. In figure 4.2 the red area in the center of the surface indicates the emission tip. The presence of an adatom in this area will change the work function of tip and this has an immediately effect on the size of the emission current. After a period of time the adatom we assume that the contamination will evaporate and the model will place the adatom at the border of the system. The model has a base emission current defined when no adatoms are present in the red area. The presents of each adatoms in this area will increase the simulated emission current while it is present. To control this extension there are several configuration options added:

- **tip**, when switched off the tip and the surrounding box can be disabled.
- **burn**, will draw a circle around the tip where the diffusivity of the adatoms is 5 times higher then normal.

- **lifetime-contamination** described the time an adatom will be on the tip before it will have enough energy to evaporate.
- **tip-full**, when turned on, the adsorption sites on the tip get the possible sites on the tip could become utilized by the presence of adatoms.
- **particle-retour**, when turned on the evaporated adatoms at the tip will be placed back at a random site at the sides of the system.

Compare simulation results with emission measurement

With the help of a UHV 300 STM system from RHK Technology the emission current over time of a carbon nanotube tip is recorded. Due to the adatoms present on the surface of the carbon nanotube the emission current will be very unstable, the tip has to be heated to make the adatoms more mobile and evaporate them from the active area of the carbon nanotube.

A small part of the measured field emission current is shown in figure 4.3. The second figure shows the results of the simulated emission current based on our model which suggest that surface diffusion is the main cause of the instability of the surface diffusion. Both signals shown the same step-like behavior, where the signal is stable for a certain period of time and then steps to a new current level. In our model the steps are caused by adatoms which move into the active area of the emitting tip, the adatom will change the tips geometry and therefore the work function. This will directly result in a change of the emission current.

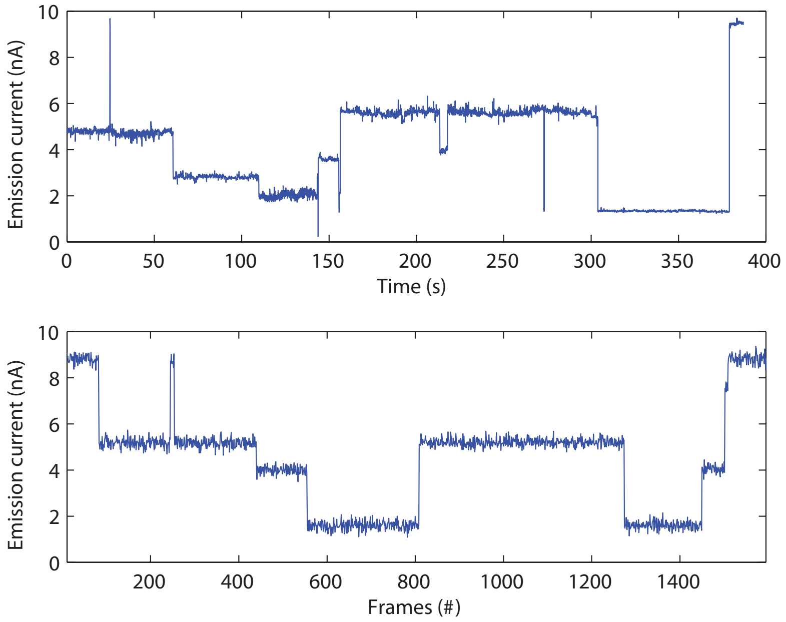

Figure 4.3: Emission current measured (above) and simulated (below)

In our model the adatoms entering the active emission area of the tip will evaporate. Over time the simulated emission current becomes more stable and less steps will occur. In figure 4.4 (left) the amount of steps during a fixed interval of time is shown. As shown in the figure the amount of transitions in the emission current is decreasing over time. The same analysis is applied on the results of the STM measurement and the result is is shown in figure 4.4 (right).

During measurements the tip is heated by the relatively large current running through the narrow carbon nanotube. The temperature of the nanotube rises and will increase the movement of the adatoms

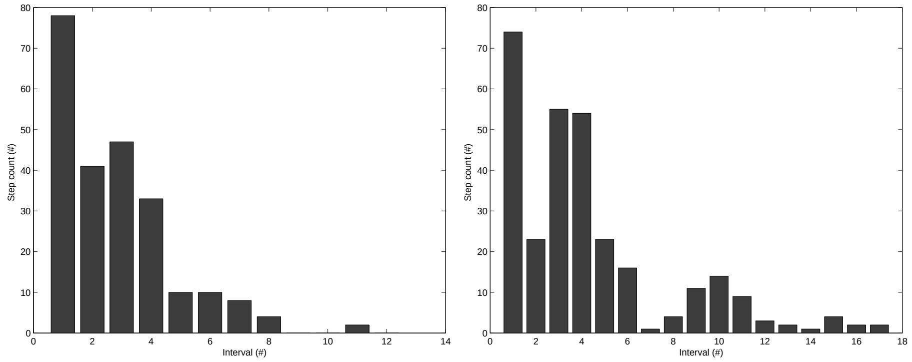

Figure 4.4: The amount of steps in the field emission current for a given period of time. Both the simulated (left) and measured (right) signal are shown.

and eventually some will evaporate of the surface and will merge with the vacuum. During operation the field emitter becomes more stable. Another applied method is using an external heat-source to clean the field emitter before operation [10]. Both applied emission currents show similar behavior. The decrease of the amount of transitions per period will result in an increase of the field emission stability.

Chapter 5

Measurements

5.1 Distance dependence field emission

As explained in the theory the amount of current during field emission depends on the distance and voltage between the conducting tip and sample. This relation is described in the Fowler Nordheim theorem and will be used to determine the field enhancement factor and the emission area of the different tips.

5.1.1 Fowler Nordheim current-voltage measurements

The current-voltage measurements are preformed for different tip-sample distances. The measurements are carried out in the RHK STM in a UHV environment. The pressure inside the chamber lies around $5 \cdot 10^{-9}$ mbar. Three distance dependent I-V measurements were taken. Each measurement was carried out with a different tip, one high-aspect ratio silicon tip and two silicon tips which are extended with a single carbon nanotube of different lengths. Each tip has an unique code and their specific characters can be found in the appendix. The results of each measurement will be treated below

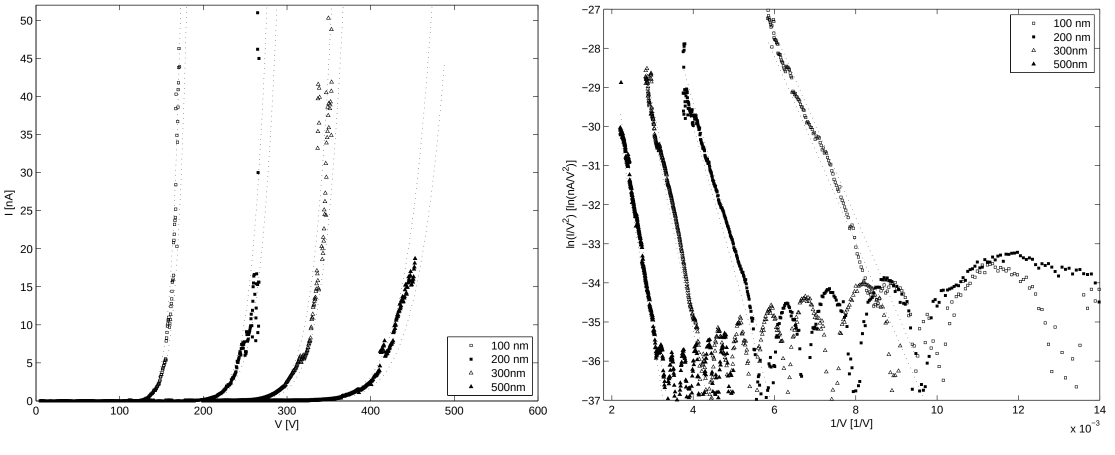

Figure 5.1: Distance dependence I-V characteristics of the field emission measured for tip-sample distances from 100 nm to 500 nm. The silicon fixed-tip is coated with 50 nm layer of molybdenum and the silicon sample is coated with $Ti_{10\%}W_{90\%}$. (left) The points represent the raw datapoint whereas the dotted lines are the result of a fitting procedure. (right) semi-logarithmic Fowler-Nordheim plot the linear shape confirms that the measured current is the result of field emission. tip: *HARA*

In figure 5.1 the I-V curve is shown for the fixed-tip coated with molybdenum. When the tip-sample distance increases a higher extraction voltage is needed to obtain the same emission current. In the left plot of figure 5.1 the leftmost curve is for the smallest tip-sample distance, where the rightmost curve has the largest tip-sample distance. The extraction voltage for a tip-sample distance of 100 nm lies at 120 V. Fowler Nordheim describes a exponential relationship between the emission current and the voltage across the tip and sample. This is caused by the chance of the field enhancement factor which increases when the tip-sample distance increases. A semi-logarithmic representation of the I-V curve is shown on the right in 5.1 when the measured currents have a linear behavior in this plot it confirms that the measured currents are the result of field emission. This linear property will later be used to determine the field emitters parameters. [3]

In figure 5.2 the I-V characteristic curve for the carbon nanotube field emitter is shown. It can be seen that the extraction voltage lies much lower then the previous tip. This is mainly because of the high-aspect ratio (length versus diameter) of the tip. The carbon nanotube *CNTHAR1* has a length of almost 220 nm an has an extraction voltage of 24 V at a distance of 50 nm.

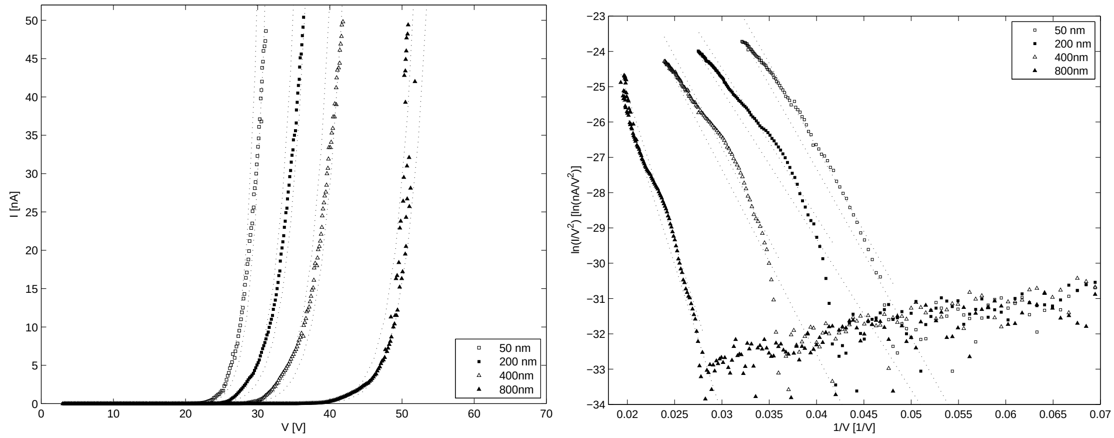

Figure 5.2: Distance dependence I-V characteristics of field emission measured for tip-sample distances from 50 nm to 500 nm. The tip consists out of a single-wall carbon nanotube positioned on the conducting tip of a silicon fixed-tip and the silicon sample is coated with $Ta_{10nm}Pt_{50nm}$. (left) The points represent the raw data points whereas the dotted lines are the result of a fitting procedure. (right) semi-logarithmic Fowler Nordheim plot the linear shape confirms that the measured current is the result of field emission. tip: *CNTHAR1*

In figure 5.3 the result of the current-voltage measurements with the carbon nanotube tip *CNTHAR2* are shown . The carbon nanotube mounted on top of the conducting silicon tip is 70 nm long. For a tip-sample distance of 50 nm the extraction voltage is 48 V.

The linear Fowler-Nordheim relation shown in the semi-logarithmic representations is used to determine several field emission parameters, like the field enhancement factor γ and the emission area A. A fitting algorithm described by le Fèbre is used to determine the parameters. The calculated factors can be found in table 5.1 [3]

Table 5.1: Field emission parameters of used tips for certain tip-sample distance

Tip	Distance (nm)	Field enhancement (γ)	Tip area (m^2)
HARA	500	4.39	$3.2016 \cdot 10^{-17}$
CNTHAR1	600	40.73	$1.5262 \cdot 10^{-14}$
CNTHAR2	600	14.46	$8.7458 \cdot 10^{-15}$

From the three measurements, it can be observed that the fixed-tip without the carbon nanotube (*HARA*) for the same tip-sample distance has a much higher extraction voltage then the tips extended

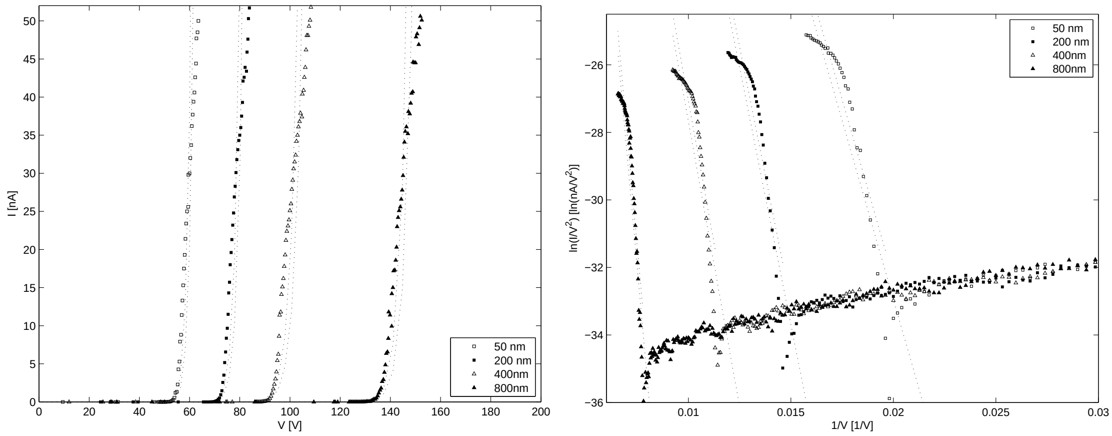

Figure 5.3: Distance dependence I-V characteristics of field emission measured for tip-sample distances from 50 nm to 500 nm. The tip consists out of a single-wall carbon nanotube positioned on the conducting tip of a silicon fixed-tip and the silicon sample is coated with $Ti_{10\%}W_{90\%}$. (left) The points represent the raw datapoint whereas the dotted lines are the result of a fitting procedure. (right) semi-logarithmic Fowler-Nordheim plot the linear shape confirms that the measured current is the result of field emission. tip: *CNTHAR2*

with a carbon nanotube (*CNTHAR1 & 2*). The estimated field enhancement factor for the tips with the carbon nanotube are much higher. This confirms the theory that the geometry of the tip has influence on the field enhancement effect. Another interesting observation is that the field enhancement factor for *CNTHAR1* is larger then *CNTHAR2*. Both have the same thickness but *CNTHAR1* is a factor of 4 times longer then *CNTHAR2*. The use of carbon nanotube makes it possible to use field emission at much lower voltages, this will result in less power consumption.

5.2 Time dependence field emission

As stated in the introduction of this report the stability and the ability to maintain it is the main challenge to overcome before field emission can be used as a precise measurement instrument. In the following experiments we will look at the effect of the use of different materials on the stability of the current and the ability to maintain it stable over time. The following different combinations of materials will be compared.

- Different tip materials hydrophobic vs. hydrophilic
- Different sample material hydrophobic vs hydrophilic
- Different tip-sample distances and location

All three different approaches will be treated below.

5.2.1 Different tip materials

In this experiment two different type of fixed-tips are used. Both are silicon coated with a conducting metal layer, but one tip is extended with a carbon nanotube. The metal coated tip has hydrophilic properties, where as the carbon nanotube has hydrophobic properties and we expect that it will be more stable and stay longer stable. As a safety measure the maximum current though the emitter is set to 100 nA, when the emission current crosses this line the software will lower the voltage. A time interval of 300 seconds of the stability measurements are shown in figure 5.4. As can be seen in the left figure the current reaches the maximum allowed current and the voltage is adjusted downwards.

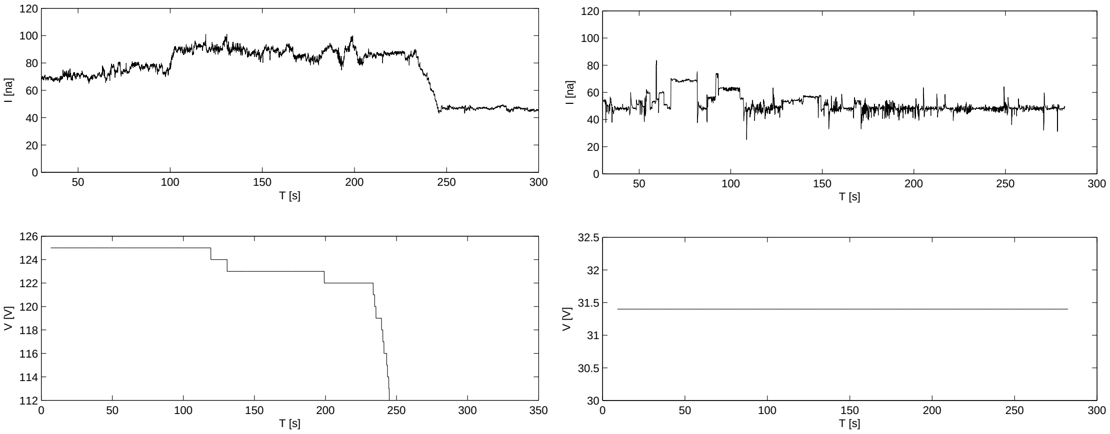

Figure 5.4: Field emission stability measurement for time interval of 300 second. In this experiment two different fixed-tip coated with 50 nm of molybdenum were used *HARA* (left). The tip in the right plot is extended with a carbon nanotube *CNTHAR1* (right). Both had a tip-sample distance of 800 nm and used the same sample material $Ti_{90\%}W_{10\%}$. The top curves show emission current as a function of time, the bottom curves show control voltage as a function of time.

5.2.2 Different sample materials

To investigate the possible contribution of the sample on the stability of field emission measurement were done with different sample materials. One sample used consists out of silicon coated with an alloy of titanium and tungsten, this metal layer gives the silicon better conducting and hydrophilic properties. The other sample is made of HOPG which consists out of thin stacked layer of carbon and has hydrophobic properties. Both measurements were carried out with the same tip and at the same tip-sample distance. Although the effect is not strong, we might conclude that the HOPG sample shows slightly better stability. Both measurements are shown in figure 5.5.

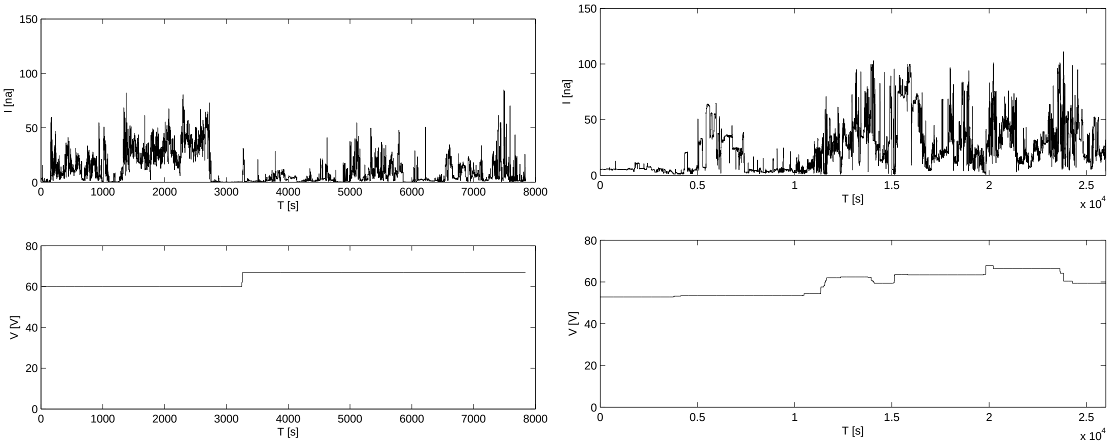

Figure 5.5: Field emission stability measurement for time interval of several hours. In this experiment two different samples were used. In the left plot HOPG is used as a sample whereas in the right plot a silicon sample coated with $Ti_{10\%}W_{90\%}$ is used. Both measurments were done with same conducting silicon fixed-tip extended with a carbon nanotube and with the same tip-sample distance of 800 nm. The top curves show emission current as a function of time, the bottom curves show control voltage as a function of time. tip: *CNTHAR7*

5.2.3 Different tip-sample distance

When the distance between the tip and the sample increase, a larger voltage is needed to get the same field emission current. In figure 5.6 two measurements are shown which were carried out at a tip-sample distance of 25 nm and 400 nm. Both experiment were carried out with the same tip and sample.

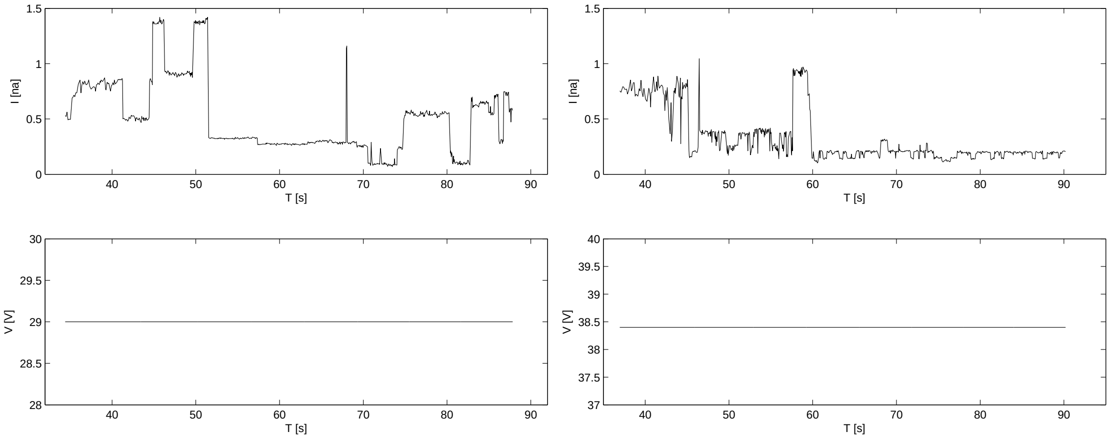

Figure 5.6: Field emission stability measurement for time interval of 300 second. This experiment was done at two different tip-sample distances of 25 nm (left) and 400 nm (right). Both measurements were done with the same carbon nanotube tip and HOPG sample. The top curves show emission current as a function of time, the bottom curves show control voltage as a function of time. tip: *CNTHAR10*

When comparing both plots it can be concluded that both have the size of the steps of instability, but the frequency at which these steps occur are much higher for the field emission current measured at a larger distance. When the distance increases, the voltage across the tip and sample also increases to maintain the same emission current. Le Fèbre showed that the active emitter sites increases when the distance increases, this means that there is a larger area where present adatoms can cause fluctuations in the emission current. [3]

5.3 Fluctuations in field emission current

During the experiments it was discovered that when measuring the field emission for a longer period of time the current will become more and more stable. The frequency of the fluctuations in the emission current decreases over time and eventually resulted in a stable situation. In figure 5.7 the result is shown of a measurement which lasted about 3 hours and eventually became stable. In the plot also a decline of the current level can be noticed, this is possible caused by the drift in the piezo actuators.

During emission continuous evaporation of adsorbents will ultimately deplete the tip surface from contaminants. The adatom will disappear in the vacuum and eventually be pumped away by the ion-pump.

In figure 5.8 a interval of a stable field emission current is shown. After three hours the emission current becomes very stable and has less then ± 7% fluctuations. These fluctuations are partly caused shot noise, junction noise and influences from the enviroment of the measurement setup. The right figure shows the frequency spectrum of the signal, unfortunately the used sample frequency of the measurement setup is only 10 Hz. So we were unable to analyse the frequency of high frequency noise sources like shot noise.

During measurements the bistable telegraph noise could also be noticed. In figure 5.9 are two measurements which shown clear signs of bistable behavior around a base emission current. The fluctuations of the emission current between two defined levels is probably caused by the same species of adatom residing in the emission area from time to time.

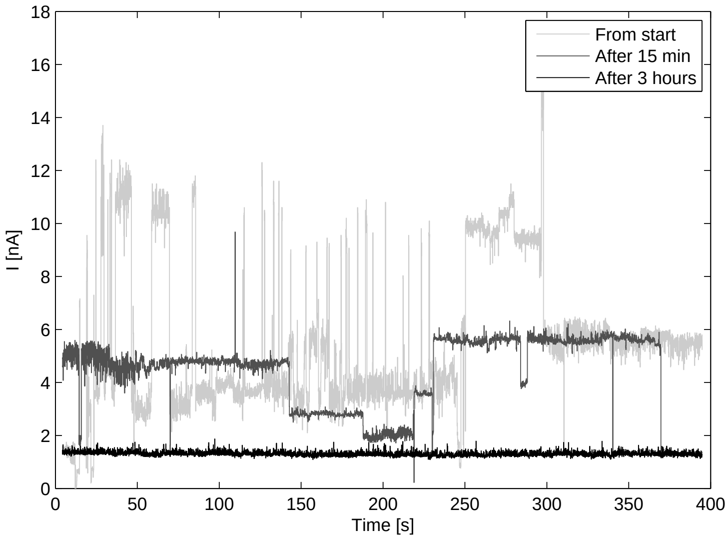

Figure 5.7: Field emission stability measurement with three samples of 300 second taking from the start, after 15 min and 3 hours of continuing field emission current. During operation the field emission stability increases tip: *CNTHAR11*. The setpoint of the emission current is 5nA, the resulting voltage 25 Volts and the tip-sample distance of 800 nm.

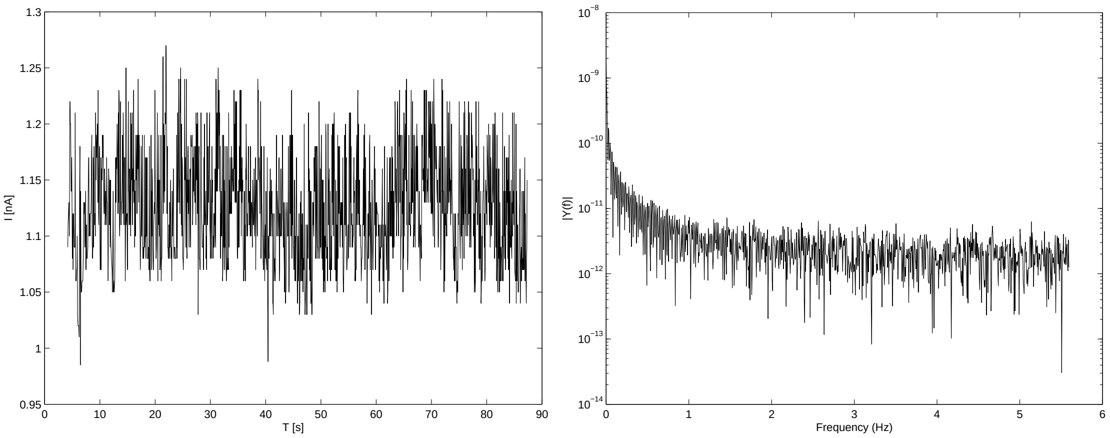

Figure 5.8: (left) Stable field emission current with less then ± 7% fluctuations in the emission current. (right) amplitude spectrum analyses of emission current.

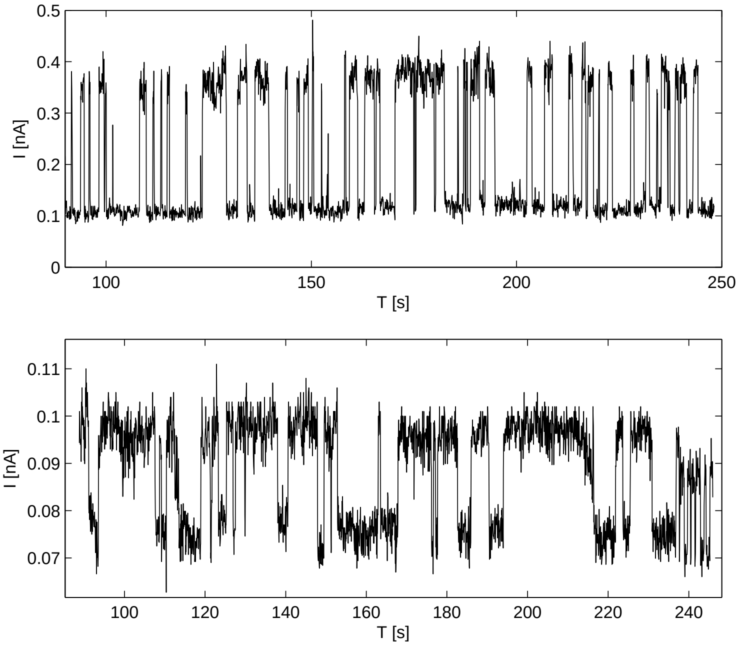

Figure 5.9: Two examples of bistable telegraph noise which occurred during several field emission measurements. These measurement were only a few minutes of continues field emission.

Chapter 6

Discussion

6.1 Material properties

6.1.1 Different tip materials

Three types of field emitters made of different materials should have been compared, but due to problems in the fabrication process only two different field emitters were actually tested. One tip is coated with a thin metal film of molybdenum and the other tip is extended with a carbon nanotube. The estimated field enhancement factor of the carbon nanotube tip is much higher then in case of the molybdenum coated tip, as expected by the theory. The field enhancement factor is enhanced by the narrow and long geometry like that of the carbon nanotube. Due to the geometry of the carbon nanotube and therefore the higher field enhancement factor the extraction voltage of the nanotube is lower then that of the tip coated with molybdenum. This is confirmed in the measurements. We expected that due to the geometry and hydrophobic character the nanotube will produce a more stable field emission, but we were not able to retrieve any conclusions from our measurement regarding the stability compared with different tip-geometries or material properties.

6.1.2 Different sample materials

The effect of the different sample materials on the surface diffusion of adatoms is reduced to a minimum when the tip-sample distance is more then a few nanometers. The field emission starts as a point source from the field emitter and then spreads outwards towards the sample. The field emission will cover a relatively large area on the sample. This area increases when the distance increases. Unlike adatoms present at the surface of the tip. Adatoms on the surface will contribute less to the fluctuation when the distance increases and maybe become unnoticeable.

6.1.3 Different tip-sample distances

Field emission measurements were done at two different tip-sample distances. As can be seen in the measurement results, the frequency of the step-like fluctuations in the emission current increases when the distance between the tip and the sample is increased. Both measurements were carried out with the same tip, sample and emission current. To obtain the same current at larger distances, a larger voltage is needed. Le Fèbre et al. explain that the active emission area of the tip increases, when the distance increase. The likelihood of a fluctuation occurring caused by an adatom increases since the area where a single adatom can effect the emission current is increased. Also more adatoms will be attracted towards the tip. The magnitude of the step-like fluctuation are the same. [3]

6.2 Field emission instability

In section 2.1.2 the three main effects for the fluctuation of the field emission current are treated. They are shot noise, bistable noise and random noise. Due to the presence of all three disturbances the accuracy and reproducibility of the measurements was to low to make hard conclusions about the influence of the different materials. Shot noise cannot be reduced because it is caused by the natural vibration of the electrons. The other two sources of instability can to reduced to a minimum, therefore all measurements were carried out in ultrahigh vacuum.

During field emission measurements for a period of time, the stability of the emission current declines. This is shown in figure 3.9 were the fluctuations in the emission current increases after it has been stable for a period of time. This observation has also been made using the conventional method were field emitters are flashed to a temperature of 1500 °C before the start of the experiment. The emission current is very stable from the start, but when time passes the frequency of the fluctuations increases until it becomes as unstable as an untreated emitter. In our case a more permanent solution has to be found since the emission current has to stay stable for a very long period of time, this means that the tip has to be cleaned actively during operation.
A possible solution is to use an external heat source to heat the emitter to 600K during a measurement, this will remove adatoms continuously and keep the surface clean. Jonge et al. demonstrated that due to continuos cleaning the fluctuations in the field emission current could be reduced to only 2-3% variation. So there are improvements here to be made in our measurement setup were no continuos cleaning is possible at this moment. [29]

Another method to clean the surface actively could be to use short highly intense current pulses. Zhu et al. demonstrated that the use of a current pulse of 1 mA for a period of 100 μs, the fluctuations in the emission current drop from 50-100% to 10%. [8]

6.3 Surface diffusion model

The Monte Carlo model describes the important role of surface diffusion on the observed fluctuations in the field emission current. The model gives us insight in the quantitative behavior of adatoms and influence of the field emission.

In the model we assume there is only one location on the tip where the presence of an adatom influences the emission current. The influence always results in the same increase in current. In practice electrons are emitted from an area instead of a point. The magnitude of a fluctuation caused by the present adatom is determined by the position of the adatom in this area and the material properties. An adatom on the top of the tip influences the current different then adatoms at the sides of the tip.

Another important observation is made when the "burn" option in the model is used for a limited period of time. When enabled, the diffusivity of the adatoms in a certain area around the emitting tip will be 5 times higher then normal. The "burn" option simulated the behavior of the adatoms at an increased surface temperature, due to higher diffusivity the total movement of the adatoms will increase and the change that these adatoms will evaporate at the tips surface will increase. The defined burn-area will be cleaned of all adatoms. In time the emission current will become stable, with some occasional spikes caused by adatom occupying the tip active area. When the "burn" option is disabled, the diffusion rate is back to normal and the emission current will become stable for a certain period of time. After a period of time it will loose its stability because large numbers of adatoms are diffusing slowly towards the tip. This phenomena has also been observed during stability measurements in previous chapter.

Chapter 7

Conclusions and recommendations

7.1 Conclusions

In the course of this project a lot of work on different areas have been done to investigate and improve the stability of field emission. The theory of field emission, causes of instabilities, the fabrication of field emitters of different materials, distance and time dependent field emission measurements were done in an ultrahigh vacuum environment and the modeling of the causes the fluctuations in the field emission current. The results of our research are summarized below.

- The field emission current is never stable from the beginning of a measurement. At the start, the presence of adatoms on the apex of the field emitter will cause fluctuations in the current. It has been recorded that during operation, the frequency of the fluctuations decreases and the field emission becomes stable with less then ± 7% of fluctiations. Here a closed cap nanotube was used as the field emittor, it would be very interesting to inspect the nanotube field emitter after measurements in a TEM to see if it still is closed cap.
- In terms of stability better results were obtained with a hydrophobic sample, then with a hydrophilic sample. Due to a fabrication problem only two different field emitters could be compared and no conclusion could be drawn about the influence of the use of hydrophobic and hydrophilic materials as field emitters.
- The fabricated field emitters showed that the extension of a metal-coated silicon tip with a carbon nanotube enhances its field emission properties. The extraction voltage of the extended emitter is only 25 Volts compared to 200 Volts of the silicon tip, both at a tip sample distance of 200 nm. As predicted by the theory the narrow and long geometry will increase the field enhancement factor.
- The distance between the tip and sample influences the stability of the field emission current. When the distance between the tip and sample is increased, the emission area of the emitter gets bigger. This means that electrons have the possibility to emit from a larger area at the apex of the tip. This increase in area, also increases the probability of adatoms influencing the emission current. This behavior is observed during measurements at two different distances, here the measurement with the largest distance have the highest frequency of fluctuations caused by the presence of adatoms. The influence of surface diffusion at the surface of the sample materials decreases when the distance to the tip increases.
- The behavior of the instabilities in the field emission current is qualitatively described by the Monte Carlo theoretical model. No contradictions between model and measurements have been found. The results of our stability measurement show the same step-like behavior and decline in the frequency of fluctuations over time as the simulated signal. When the tip in our model is heated by an external source, the field emission becomes very stable. After the heater is turned off, the stability slowly declines and the emission current becomes as unstable at before. The same effect has been observed in several experiments.

Due to random disturbances in the field emission measurements, it is very difficult to find comparable and conclusive results that clearly expose the influence of different materials on the stability of the field emission.

7.2 Recommendations

To achieve, and more importantly: maintain stable field emission currents, some way will have to be found to actively clean the field emitter during operation. A suggestion is to use small pulses of high currents, this will heat up the tip and remove any present adatoms. Such as system could be integrated in the current measurement setup with some minor adjustments.

To gain a better insight in the macro-scale effects the surface diffusion model has to be extended. The current model uses statistical probability to determine the movement of each individual adatom, there is no interaction between the adatoms or possibility to cluster.

Appendix A

High-aspect ratio tips

A.1 Fabrication process High-aspect ratio tips

1. 4” standard wafer, 311 nm LPCVD low stress SiN
2. Litho base mask (HMDS 3000 rpm 2min hot plate 200 °C, AZ5214 5000rpm 2min 120 °C, expose 4 8sec, MF321 75sec, slightly over develop)
3. Etch ½ SiN (311/2=155 nm) CHF_3 10min
4. Cleaning + ultrasonic
5. Litho tip mask
6. Etch SiN until Silicon substrate (155nm SiN)
7. KOH full wafer 350 μm deep
8. Dice samples
9. Cleaning +ultrasonic
10. KOH etching in samples, with controlled etching until a nice plate form
11. Etch SiN until the SiN base pattern etched through and land on Si (155 nm)
12. Cleave the clamping bridge
13. Cleaning + ultrasonic + Rezi28 @75 °C (clean well)
14. Etch Si isotropically ½ circle (2.5 μm each side)
15. Etch Si anisotropically (cryogenic) SF_6 and O_2, black silicon grass will form
16. Cleaning + HF (removing side wall protection) + rezi28 (clean well)
17. Etch Si isotropically until 500 nm tip neck (removing the silicon grass)
18. Oxidation 250 nm of Si (544 nm SiO_2 total thickness) Over oxidation is possible
19. Etch backside SiN by flipping sample and with elevated loading chip (20min)
20. Etch backside Si substrate by flip-sample+loading chip (30min)
21. Release the flip-sample, cleaning+rezi28, clean well the thermal paste.
22. HF dip to remove SiO_2 and SiN pad

C.K. Yang 11-10-2008 c.k.yang@tudelft.nl

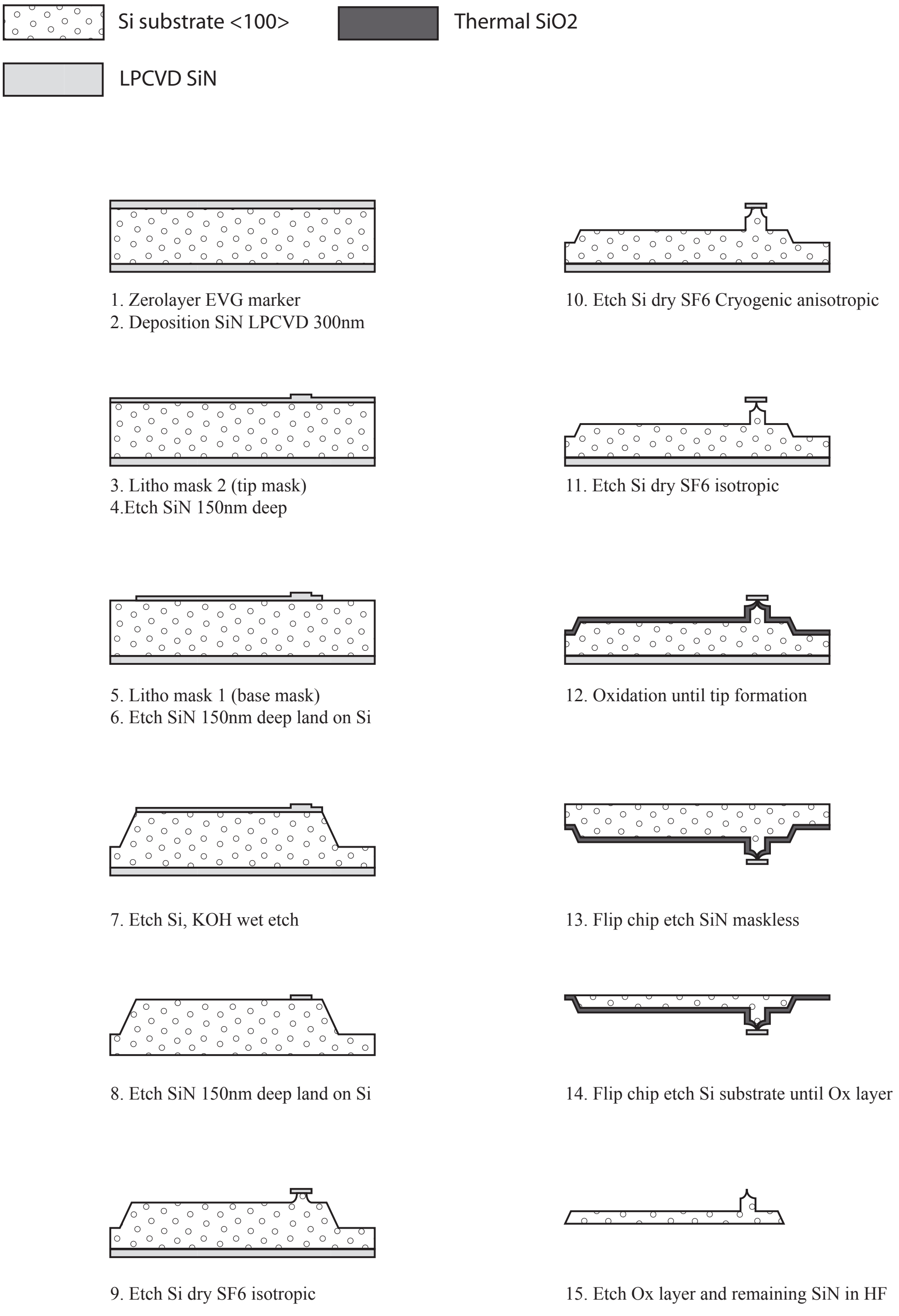

1. Zerolayer EVG marker
2. Deposition SiN LPCVD 300nm

3. Litho mask 2 (tip mask)
4.Etch SiN 150nm deep

5. Litho mask 1 (base mask)
6. Etch SiN 150nm deep land on Si

7. Etch Si, KOH wet etch

8. Etch SiN 150nm deep land on Si

9. Etch Si dry SF6 isotropic

10. Etch Si dry SF6 Cryogenic anisotropic

11. Etch Si dry SF6 isotropic

12. Oxidation until tip formation

13. Flip chip etch SiN maskless

14. Flip chip etch Si substrate until Ox layer

15. Etch Ox layer and remaining SiN in HF

Figure A.1: Fabrication process of high-aspect ratio tips out of a 4’ inch silicon wafer

Appendix B

Fabricated Field emission tips

B.1 Fabricated CNT tips

Table B.1: Settings used during experiments

Date	Name	Length tip (nm)	Deposition Pt	Comments
01-09-2008	HAR_A	9640	no	
01-12-2008	CNT_HAR_1	220	no	
01-12-2008	CNT_HAR_2	70	no	
08-12-2008	CNT_HAR_3	-	no	
08-12-2008	CNT_HAR_4	-	no	
08-12-2008	CNT_HAR_5	283	yes	
08-12-2008	CNT_HAR_6	-	no	Tip broke during fabrication
22-12-2008	CNT_HAR_7	-	no	Tip broke during fabrication
22-12-2008	CNT_HAR_8	475	yes	Tip has lot of carbon dirt
22-12-2008	CNT_HAR_9	180	yes	Nod in CNT of 30°
22-12-2008	CNT_HAR_10	472	yes	
22-12-2008	CNT_HAR_11	1080	yes	
22-12-2008	CNT_HAR_12	-	no	Tip broke during fabrication
23-03-2009	CNT_HAR_20	-	-	SiN layer could not be removed
23-03-2009	CNT_HAR_21	703.48	no	SiN layer successfully removed from tip
23-03-2009	CNT_HAR_22	-	-	SiN layer could not be removed
23-03-2009	CNT_HAR_23	384.90	yes	
26-03-2009	CNT_HAR_24	1350.00	yes	
26-03-2009	CNT_HAR_25	-	-	SiN layer could not be removed
26-03-2009	CNT_HAR_26	-	-	No silicon tip present
26-03-2009	CNT_HAR_27	-	-	Tip crashed during

Appendix C

STM Setup

C.1 Procedure to interchange the current amplifiers connected to the STM: RHK

C.1.1 IVP-200 and Keithley Picoammeter 6487

N.B. Please note that there are 2 BNC connectors to the scan head:

- Coaxial cable connected through 100 MOhm to the scanner (short BNC)
- Coaxial cable connected directly to the scanner (long BNC)

C.1.2 Connect Keithley Picoammeter 6487

- Retract tip and scanner far enough from sample to prevent tip crash, don't forget to select the z-axis on the switchboard.
- Lower bias voltages to sufficiently low value (3-5 V) on SPM1000 (P-863 HV-source) as well as Keithley 6487 for safety/damagecontrol.
- Disconnect RHK IVP-200 current amplifier from BNC connector on scan-flange and lay it aside (e.g. on top of vacuum system).
- Disconnect bias voltage cable from BNC connector on sample-table-flange.
- Disconnect cable to RHK current amplifier (grey cable) from SPM1000.
- Connect triax-to-BNC cable of Keithley 6487 to (short) BNC connector on scanner-flange.
- Connect analog-out of Keithley 6487 to BNC pre-amp input on SPM1000 and SET PRE-AMP SELECTOR SWITCH TOWARDS BNC-CONNECTOR.
- Connect V-Source output from Keithley 6487 to BNC connector on sample-table-flange. Make sure the ground is connected to the Keithley's chassis (yellow cable) to prevent oscillations in the feedback loop (reason unknown).
- SET ON SPM1000 THE BIAS-POLARITY TO - (MINUS) TO COMPENSATE FOR THE INVERTING ANALOG OUTPUT (IVP-200 is non-inverting). The bias polarity on the SPM1000 does not represent the real bias voltage on the sample, since this is set by the Keithley V-Source.
- Set the Keithley 6487 current amplifier range to 200 nA to have faster analog output (300 μs rise time). Resetting to the the correct Keithly settings can best be done by clicking "Initialize" in Keithley control software.

- SET THE CURRENT SETPOINT KNOB TO 0.3 TO HAVE 3 nA CURRENT. This difference is caused by the lower pre-amp gain (1e7) compared to the IVP-200. Using a 20 nA range would give the same gain (1e8), but a slower analog output respons (4 ms rise time).
- Set the SPM1000 control loop: gain 10 and time-constant 1 to make it sufficiently fast (flat sample). Lower gain values and higher time-constant may be required for rough samples or fast scan times.
- Set in the XPM Pro control software ("Settings" -> "Configure Hardware" -> "Gains" -> "STM current per monitor volt") the amplifier-gain to 100 nA (per Volt) so that the software reads the correct current values.
- Test the new settings by approaching the tip to the sample and make some test scan lines. Read the Keithley 6487 display to see if the correct current setpoint is reached. If a too high value is displayed, the tip is probably crashed, resulting in a maximum current of the set bias voltage divided by 100 MOhm (current-limiting resistor). If not, you followed this guide very well ;).

C.1.3 Connect RHK-IVP200

- Retract tip and scanner far enough from sample to prevent tip crash, , don't forget to select the z-axis on the switchboard.
- Lower bias voltages to sufficiently low value (3-5 V) on SPM1000 (P-863 HV-source) as well as Keithley 6487 for safety/damagecontrol.
- Disconnect triax-to-BNC cable of the Keithley 6487 from BNC connector on scan-flange.
- Disconnect V-source output of Keithley 6487 cable from BNC connector on sample-table-flange.
- Disconnect analog out Keithley 6487 from the BNC pre-amp input on SPM1000.
- Connect RHK IVP-200 current amplifier to the (short) BNC connector on scanner-flange.
- Connect RHK IVP-200 (grey cable) to the input of the SPM1000 and SET PRE-AMP SELECTOR SWITCH TOWARDS THE CONNECTOR.
- Connect the output of the voltage amplifier ("Piezo Controller" to the BNC connector on sample-table-flange.
- SET ON SPM1000 THE BIAS-POLARITY TO + (PLUS), because the IVP-200 is non-inverting.
- SET THE CURRENT SETPOINT KNOB TO 3 nA CURRENT.
- Set the SPM1000 control loop: gain 2 and time-constant 7 to make it sufficiently slow to suppress possible resonances.
- Set in the XPM Pro control software ("Settings" -> "Configure Hardware" -> "Gains" -> "STM current per monitor volt") the amplifier-gain to 10 nA (per Volt) so that the software reads the correct current values.
- Test the new settings by approaching the tip to the sample and make some test scan lines. Read the SPM1000 display to see if the correct current setpoint is reached. If a too high value is displayed, the tip is probably crashed, if not you are a genius :)

Bibliography

[1] C. Yang, A. le Fèbre, G. Pandraud, E. van der Drift, and P. French, “Field emission for cantilever sensors,” *Journal Vacuum Science Technology*, vol. 26, pp. 927–930, 2008.

[2] H. Busta, J. Pogemiller, and B. Zimmerman, “The field emitter triode as a displacement/pressure sensor,” *Journal Micromechanics* & *Microengineering*, vol. 3, 1993.

[3] A. le Fèbre, *Field emission sensing for non-contact probe recording.* Koninklijke Wöhrmann, 2008.

[4] R. Wood, “A new form of cathode discharge and the production of x-ray,” *Physical Review Papers*, vol. 5, pp. 1–10, 1897.

[5] W. Schottky, “Uber kalte und warme elektronenentladung,” *Zeitschrift fur Physik A: Handrons und Nuclei*, vol. 14, pp. 63–106, 1923.

[6] R. Fowler and L. Nordheim, “Electron emission in intense electric fields,” *Proceedings of the Royal Society of London, Containing Papers of a Mathematical and Physical Character*, vol. 119, pp. 173–181, 1928.

[7] G. Kusne, *Instrument for Characterization of Field Emission Properties of Nanostructured Surfaces.* Cargenie Mellon University, 2005.

[8] W. Zhu, *Vacuum Microelectronics.* John Wiley & Sons, 2001.

[9] A. le Fèbre, L. Abelmann, and C. Lodder, “Field emission at nanometer distances for high-resolution positioning,” *Journal Vacuum Science Technology*, vol. 26, pp. 724–728, 2008.

[10] G. Antczak, “Jump processes in surface diffusion,” *Surface Science Reports*, vol. 62, pp. 39–61, 2006.

[11] R. Ferrando, “Surface diffusion: Simulation,” *Elsevier*, pp. 1–6, 2006.

[12] M. I. Larsson, “Surface diffusion mechanism for step bunching,” *Physical review*, vol. 56, pp. 157–166, 1997.

[13] D. C. Senft, “Atomic jump lengths in surface diffusion: experiment and theory,” *Applied Surface Science*, vol. 94, pp. 231–237, 1996.

[14] M. Dresselhaus and G. Dresselhaus, “Nanotechnology in carbon materials,” *Nanostructured materials*, vol. 9, pp. 33–42, 1997.

[15] P. Avouris and J. Chen, “Nanotube electronics and optoelectronics,” *Materials Today*, vol. 9, no. 10, pp. 46–54, 2006.

[16] M. Meyyappan, L. Delzeit, A. Cassell, and D. Hash, “Carbon nantube growth by pecvd,” *Plasma sources science and technology*, vol. 12, pp. 205–216, 2003.

[17] H. Dai, “Carbon nanotubes: Synthesis, integration and properties,” *Accounts of chemical research*, vol. 35, pp. 1035–1044, 2002.

[18] S. Iijima, “Helical microtubules of graphitic carbon,” *Nature*, vol. 354, pp. 56–58, 1991.

[19] J. Appenzeller and el., “Carbon nanotubes as potential building block for future nanoelectronics,” *Microelectronic Engineering*, vol. 64, pp. 391–397, 2002.

[20] T. K. M. Yudasaka and S. I. T. Ichihashi, “Single-wall carbon nanotube formation by laser ablation using double-targets of carbon and metal,” *Chemical Physics Letters*, vol. 278, pp. 102–106, 1997.

[21] T. Charinpanitkul, W. Tanthapanichakoon, and N. Sano, “Carbon nanostructures synthesized by arc discharge between carbon and iron electrodes in liquid nitrogen,” *Current applied physics*, vol. 9, pp. 629–632, 2009.

[22] C. Bower, W. Zhu, S. Jin, and O. Zhou, “Plasma-induced alignment of carbon nanotubes,” *Applied Physics Letters*, vol. 77, no. 6, pp. 830–832, 2000.

[23] J. de Vries, “Field emission from carbon nanotubes in uhv conditions,” 12 2008, university of Twente.

[24] A. Rinzles, J. Hafner, P. Nikolaev, L. Lou, D. Tomanek, P. Nordlander, D. Colbert, and R. Smalley, “Unraveling nanotubes: Field emission from an atomic wire,” *Science*, vol. 269, 1995.

[25] “Rosseter holdings limited,” Internet.

[26] “Rhk technology inc. rhk uhv 300,” Internet.

[27] “Keithley instruments inc. - keithley 6487 picoammeter/voltage source,” Internet.

[28] N. University, “Netlogo home page,” http://ccl.northwestern.edu/netlogo/.

[29] N. de Jonge, M. Allioux, J. T. Oostveen, K. B. K. Teo, and W. I. Milne, “Optical performance of carbon-nanotube electron sources,” *PHYSICAL REVIEW LETTERS*, vol. 94, pp. 2247–2249, 2005.